INVESTIGATING CRUSTAL STRUCTURE OF THE MARMARA REGION USING LOCAL TOMOGRAPHY AND SEISMIC ANISOTROPY METHODS

by

Gülten Polat

B.S., Geophysical Engineering, Dokuz Eylül University, 2000

M.S., Geophysics, Boğaziçi University, 2006

Submitted to the Kandilli Observatory and
Earthquake Research Institute in partial fulfillment of
the requirements for the degree of
Doctor of Philosophy

Graduate Program in Geophysics

Boğaziçi University

2019

ACKNOWLEDGEMENTS

As first, I want to give my deep gratitude to my supervisor Prof. Dr. Nurcan Meral Ozel for her infinite aid to my research. Her guidance strongly assisted me during all the time of research and writing of this thesis. It is always a pleasure to be one of her students and work with her during all my life. I am deeply grateful to Prof. Dr. Niyazi Turkelli from geophysics department at Bogazici University, Geophysics Department, Kandilli Observatory and Earthquake Research Institute (KOERI) for enlightening me the first glance of research and suggestions, guidance and support during my Ph.D. study. Also, I want to thank all staffs from National Earthquake Monitoring Centre (NEMC) and The Scientific and Technological Research Council of Turkey (TUBITAK) for supporting me collecting data. My special thanks are to Ivan Koulakov from Trofimuk Institute of Petroleum Geology and Geophysics, SBRAS, Prospekt Koptyuga for permission to use his tomography code LOTOS. My other special thanks are to my best friends Mehtap Erberk, Zeynep Yılmaz, Nilay Başarır, Seda Yelkenci, Ugur Teoman, Tugce Afacan, Dogan Aksarı and Alper Denli for their immense patience, support, comments, and friendship.

Finally, I am grateful to my family, especially my mom Seringul, my older brother Orhan and my sisters Bahar and Akgul Polat for helping me with complete confidence during my lifetime. I know, without their patience, support, and understanding, it would not be possible for me to complete my thesis.

Dedicated to my younger brother, RAMAZAN POLAT

ABSTRACT

INVESTIGATING CRUSTAL STRUCTURE OF THE MARMARA REGION USING LOCAL TOMOGRAPHY AND SEISMIC ANISOTROPY METHODS

The crustal structure underneath the Marmara region was investigated by utilizing local tomography and shear wave splitting methods in this study. These regions have high seismicity and are thus of serious importance to seismic risks. The first part of the research was based on travel-time tomography utilizing local moderate and microseismic events occurring in the study area recorded by the Multi-Disciplinary Earthquake Research in High-Risk Regions of Turkey project and Kandilli Observatory and Earthquake Research Institute. We had chosen 2,131 seismic events and 92,858 arrival times in total, comprising of 50,044 P-wave and 42,814 S-wave arrival times. The mapped earthquakes were gathered in the segments of the fault that has high seismicity. Low velocities were observed beneath the central Marmara Sea at 5 km depth. Also, the 2006 Mb =5.3 Manyas-Kus Golu (Manyas) earthquake had been retrospectively "stress-forecasted" utilizing changes in time-delays of seismic shear wave splitting to evaluate the time and magnitude at which tension-modified microcracking reaches fracture criticality within the stressed volume where strain is released. We observed that clear decreases in delay-times before the impending event, especially at the station GEMT are consistent with the anisotropic poroelasticity (APE) model of fluid-rock deformation, but we could not observe similar changes at other stations surrounding the main event. The logarithms of the duration of the tension accumulation are proportional (self-similar) to the magnitude of the impending event. Although time and magnitude of the 2005 Manyas earthquake could have been stress-forecasted, as has been recognized elsewhere, shear wave splitting does not appear to provide direct information about the location of impending earthquakes.

ÖZET

LOKAL TOMOGRAFİ VE SİSMİK ANİZOTROPİ YÖNTEMLERİNİ KULLANARAK MARMARA BÖLGESİNİN KABUK YAPISINI ARAŞTIRMAK

Bu çalışmada, lokal tomografi ve kayma dalgası ayırma yöntemleri kullanılarak Marmara bölgesinin kabuk yapısı incelenmiştir. Bu bölgeler yüksek sismikliğe sahiptir ve bu nedenle sismik riskler için ciddi öneme sahiptir. Seyahat süresi tomografisine dayalı ilk olan bu kısmında; Türkiye'nin Deprem Riski Yüksek Jeo-Stratejik -ancak tektonik rejimleri farklı- Bölgelerinde Deprem Davranışının Çok Disiplinli Yaklaşımlarla Araştırılması (TÜRDEP) Projesi kapsamında kurulan sismik istasyonlar ile Kandilli Rasathanesi ve Deprem Araştırması istasyonları tarafından bölgede kaydedilen lokal orta ve mikro depremler kullanılmıştır. 50.044 P ve 42.814 S dalgası'nın toplamda oluşturduğu 92.858 varış zamanının üretildiği, 2.131 deprem seçildi. Haritalanan depremler, yüksek sismisiteye sahip fay segmentlerinde kümelenmiştir. 5 km derinlikte, Marmara Denizi'nin merkezi altında düşük hızlar görülmüştür. Ayrıca, 2006 Mb=5.3 Manyas-Kuş Golu (Manyas) depremi retrospektif olarak "stres-tahmin" edilmesi için; modifiye edilmiş stresten kaynaklı mikro çatlakların gerilme hacminin gerginliğin arttığı hacim içinde kırılma kritikliğine ulaştığı zaman ve büyüklüğü değerlendirmesi, sismik kesme dalgası bölünmesinin zaman gecikmelerindeki değişimler kullanılmıştır. Bu deprem öncesinde, özellikle GEMT istasyonunda, gecikme sürelerinde belirgin düşüşler gözlemledik, bu da, sıvı-kaya deformasyonunun anizotropik poroelastisite (APE) modeli ile uyumludur. Ancak, bu depremin yakın çevresindeki diğer sismik istasyonlarda benzer değişiklikleri gözlemleyemedik. Stres birikimi süresinin logaritmaları, olması muhtemel olan deprem büyüklüğü ile orantılıdır yani kendine hastır. Kesme dalgası ayrımlanması yöntemi ile, 2005- Manyas depreminin zaman ve büyüklüğü stres değişiminden öngörülse de, depremin lokasyonu hakkında bilgi üretilememiştir.

TABLE OF CONTENTS

LIST OF FIGURES

LIST OF TABLES

LIST OF SYMBOLS

δt	Delay time
ϕ	Fast polarization direction

LIST OF ACRONYMS/ABBREVIATIONS

2D	Two Dimensional
3D	Three Dimensional
AB	Antalya Basin
AFAD	Prime Ministry Disaster and Emergency Management Authority, Republic of Turkey
APE	Anisotropic Poro-Elasticity
BB	Broadband Period stations
EAF	East Anatolian Fault
EAP	Eastern Anatolia Plateau
EBSB	Eastern Black Sea Basin
BS	Bitlis Suture
CA	Cyprus Arc
HA	Hellenic Arc
IA	Isparta Angle
IZ	Istanbul Zone
KOERI	Bogazici University, Kandilli Observatory and Earthquake Research Institute
KTJ	Karlıova Triple Junction
LET	Local Earthquake Tomography
LOTOS	Local Tomography Software
MM	Menderes Massif
NAF	North Anatolian Fault
NEMC	National Earthquake Monitoring Centre
NMT	North Marmara Through
OBSs	Ocean-bottom seismometer
SH	Short Period stations
TB	Thrace Basin
TUBİTAK	Scientific and Technological Research Council of Turkey

TURDEP	Multi-Disciplinary Earthquake Research in High Risk Regions of Turkey project
WBB	Western Black Sea Basin

1. INTRODUCTION

Throughout history, many devastating earthquakes such as August 17 and November 12, 1999, earthquakes occurred in the Marmara region. Their magnitudes are Mw=7.5 and Mw=7.2, respectively. According to geological and geophysical studies (e.g., Ambraseys, 2002; Karabulut et al., 2003), the region is one of the most seismically active areas in the world. Although many earth scientists investigate this area with different geophysical and geological tools such as local tomography, the detailed crustal structure of the study area is not yet known. The main subject of interest is how present-day and past dynamical processes within the Marmara region have evolved through time. Knowledge about this question is currently limited. In particular, microearthquake activities and its source mechanisms in the Marmara Sea are also not known well. Therefore, this region is still tectonically and geologically investigated. Considering the tectonic and geologic structure of the study region, it may be seen that particularly the North Anatolian Fault (NAF) plays a significant role in its tectonic evolution. Therefore, our study area is extended to cover the western segments of the NAF. After the last devastating earthquakes, a large number of broadband stations were installed in Turkey and particularly in the Marmara region. Therefore, we were able to collect a strong dataset recorded by stations of Bogazici University, Kandilli Observatory and Earthquake Research Institute (KOERI) and the Scientific and Technological Research Council of Turkey (TUBITAK) during the Multi-Disciplinary Earthquake Research in High Risk Regions of Turkey project (TURDEP) to investigate the crustal structure of the Marmara region and surrounding areas by using local tomography and shear wave splitting methods.

1.1. The Structure of The Thesis

In the thesis, firstly a geological overview of the Marmara region and surrounding areas is given in chapter 2, in particular, the tectonic evolution of the NAF. This chapter also includes previous geological and geophysical studies done in the study area. In chapter 3, information about instruments and collected data is given in de-

tail. Relocation processing of the collected data is also given in the chapter. Detailed information about the quality of data is discussed in this chapter. Local tomography method is described in chapter 4. Then, results obtained from this method are presented in chapter 4. In addition to this method, shear wave splitting method is utilized in this study. In chapter 5, the splitting method, and its results are given. In chapter 6, the derived results from both the methods are discussed and the thesis concludes with a summary of the study and the main conclusions drawn from the local tomography and shear-wave splitting analysis.

2. GEOLOGICAL AND GEOPHYSICAL BACKGROUND

As first, the early and present geologic history of the Anatolian plate will be summarized in this chapter. Then, the geologic and tectonic structure of the study region will be reviewed and detail information about previous geological and geophysical studies carried on the Marmara region will be also be presented.

2.1. Geological Background

Looking at the geological past of the Anatolian plate, it has been fundamentally formed between the two mega-continents: Gondwana to the south and Laurasia to the north. The Eurasian and also the Arabian–African plates have enforced a pushing pressure to the Anatolian plate (e.g., Şengör and Yılmaz, 1995) (Figure 2.1). As a result of these interactions between the plates, the Anatolian plate is moving westward relative to Eurasia in eastern Turkey at roughly 40 mm/yr (Pichon et al., 1995), however, starts moving southwesterly in western Turkey (Jackson, 1994). An interplay of this movement and also the geological process of the Mediterranean layer to a lower place the Turkish plate causes a N-S expansion and E-W shortening in western Turkey. As a consequence of this, the area is underneath expansion in a NNE-SSW direction. Also, recent geodynamic researches (e.g., Hippolyte et al., 2016) indicated that the present geodynamic structure of the Anatolian plate has been ruled by tectonic interactions between the plates and the ongoing internal deformation along their boundaries. Additionally, staring at the tectonic structure of Turkey, Turkey lies at intervals the Alpine-Himalayan orogenic zone. The findings of Göncüoğlu (2010) indicated that Early Tertiary is the time of Alpine collisional period and accompanied by the generation of the big post-transtensional and transpressional basins. The interactions cause a large variety of complex tectonic processes like collision, subduction, back-arc extension, strike-slip faulting and rotation of different blocks and microplates at intervals a comparatively little region.

Figure 2.1. A simplified tectonic map of Turkey and surroundings. (AB) Antalya Basin; (BS) Bitlis Suture; (EAF) East Anatolian Fault; (EAP) Eastern Anatolia Plateau; (EBSB) Eastern Black Sea Basin; (IA) Isparta Angle; (HA) Hellenic Arc; (CA) Cyrus Arc; (IZ) Istanbul Zone; (MM) Menderes Massif; (NAF) North Anatolian Fault; (TB) Thrace Basin; and (WBB) Western Black Sea Basin.

As indicated in Figure 2.2, many oceanic and continental "terranes" with distinct geological components formed the Anatolian plate. In particular, the present dissemination of the terranes is associated with the closure of various Neotethyan branches.

Turkey is geologically divided into three main tectonic components: the Pontides, the Anatolides-Taurides and the Arabian Platform (Ketin, 1966). These tectonic components, which were encompassed of oceans in the past, are now separated by sutures, which mark the tectonic lines or zones along which these oceans have been lost (Okay, 2008) (Figure 2.3). The closure of the Neotethyan oceanic basins in the Turkish region; namely the Intra-Pontide, Izmir-Ankara, and Amanos Elazıg-Van-Zagros oceanic basins, has resulted in the emplacement of the oceanic-accretionary prism complexes towards south onto the passive margins of the Sakarya, Tauride-Anatolide and SE

Anatolian micro-plates, respectively (Göncüoğlu, 2010).

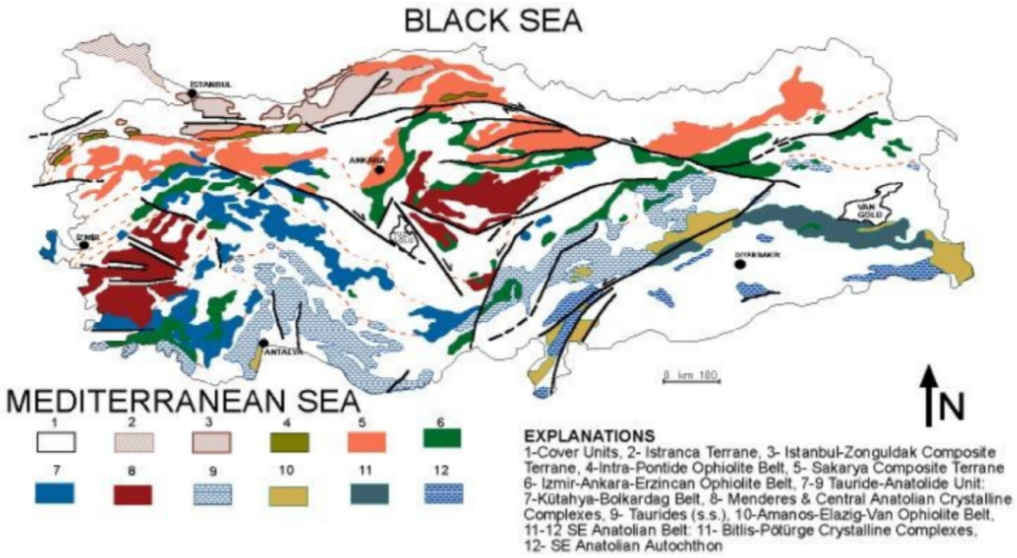

Figure 2.2. The primary Alpine terranes formed in Turkey (Göncüoğlu et al., 1997).

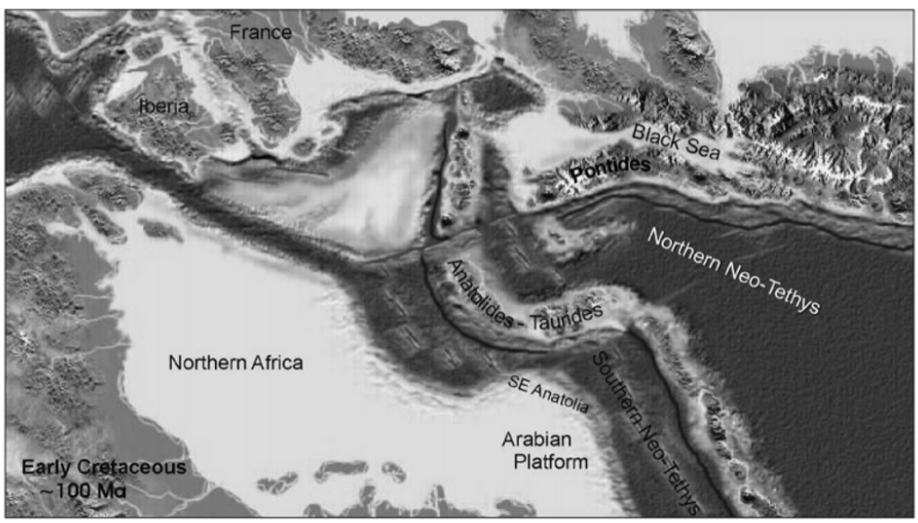

Figure 2.3. A view of the Mediterranean palaeogeography during the Early Cretaceous (110 Ma). Note the absence of Anatolia as a single landmass (taken from Okay (2008)).

As stated by Göncüoğlu (2010), the development of this tectonic structure is identified with the formation fore-land and fore-deep type flysch basins, where tectonic

slices allochthonous oceanic material (ophiolite complexes, blueschist facies metamorphic rocks) jointly with slices of the ancient continent margin accumulations (mostly old slope deposits) were established for tens of kilometers onto the passive margins during the latest Cretaceous-Early Tertiary period. Görür and Tüysüz (2001) indicated that this has been maintained by the formation of countless molasses-type basins in Anatolia during the Paleogene time. According to plate tectonic theory in the vicinity of the Anatolian block, the Eurasian, the African and the Arabian plates border each other. The relative movement of these plates (Figure 2.4), mainly dominate the present tectonic regime and the seismicity of Turkey.

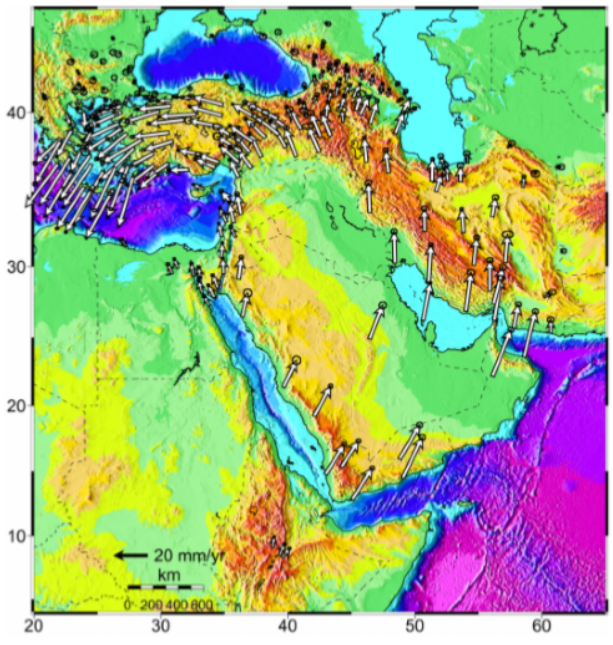

Figure 2.4. This map exhibits decimated GPS velocities comparative to Eurasia determined by Reilinger (2006).

Northward movement of the Arabian plate in respect to the Eurasian plate causes a lateral escape of the Anatolian block toward the west and the northeastern block toward the east, resulting in right lateral movement along the NAF, which is the boundary in the middle of the Eurasian and Anatolian plates and left-lateral movement along the EAF, which is another transform boundary in the middle of the Anatolian and the Arabian plates (McKenzie, 1972; Dewey and Şengör, 1979). It suggests that

the Eurasian and Arabian–African plates enforced a pushing pressure to the Anatolian plate (Şengör and Yılmaz, 1981). All studies indicate that this force is continuing. As a consequence of these, intensive pushing pressures against the Anatolian plate, the seismically active NAF and EAF were developed in the plate. As shown in Figure 2.5, these two main fault systems are conjugated in Karlıova.

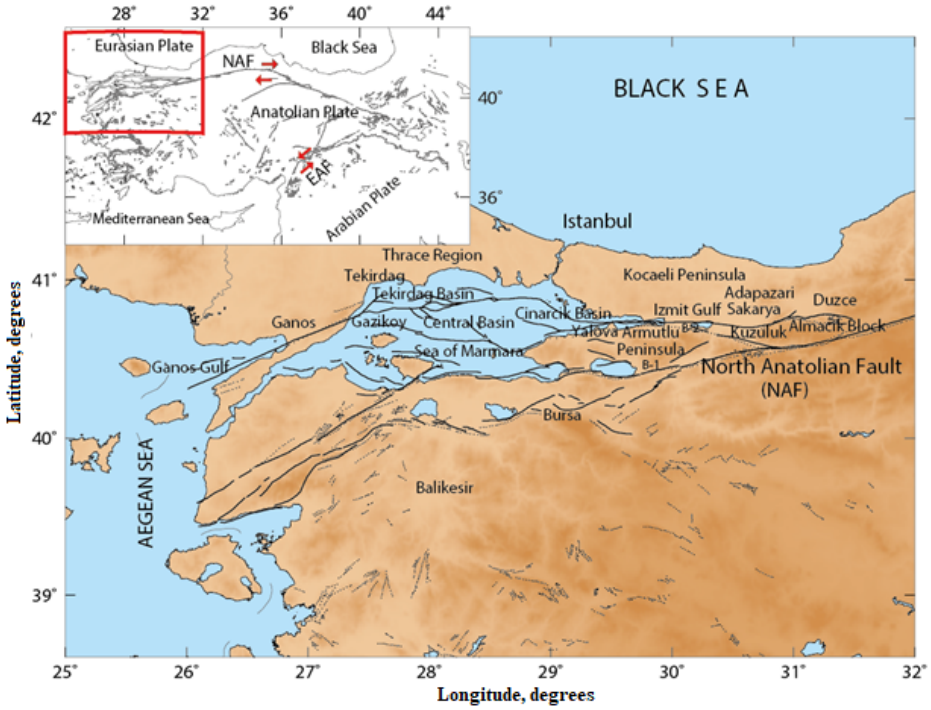

Figure 2.5. This map shows the primary tectonic units developed in the study area (dot black faults from Şaroğlu (1987), thick black faults from Armijo (1999). Inset: The location of the study area within Turkey is marked red. (KTJ) Karlıova Triple Junction; (EAF) East Anatolian Fault and (NAF) North Anatolian Fault.

The NAF is one of the major continental transform faults in the world. It is also the main boundary in the middle of the Anatolia and Eurasia plates and extends E-W across Turkey for over 1600 km (see Figure 2.5). The right-lateral, the absolutely strike-slip tectonic regime that characterizes the NAF over its eastern part from the Karliova Triple Junction (KTJ) splays in the Sea of Marmara region into three main fault segments, the Northern, the Middle and the Southern strands (Barka, 1992). The Northern and the Middle branches bound the Sea of Marmara (see Figure 2.5). The

NAF poses a significant seismic risk for the big cities around the Sea of Marmara, especially Istanbul. In present, the NAF is hosting along an undeformed branch underneath the Marmara Sea (Schmittbuhl et al., 2015). Geologic studies (e.g., Smith et al., 1995) indicated that the Sea of Marmara is located in a transition zone where the right-lateral strike-slip character of the NAF meets with the extensional character of Aegean. In the Eastern Sea of Marmara, a transition region happens from the right lateral strike-slip to the Aegean expansion zone (Armijo et al., 2005). In the light of the above, it could be said that the Marmara region is located in the NAF system. The mentioned above system in the middle of the Bosphorus and the Dardanelles is generally defined as a transition region between the strike-slip regime of the NAF to the east, and the expansion regime of the Aegean Sea to the west (e.g., Gürbüz et al. 2000). Tectonic units in the area are characterized by the splitting of the NAF into three segments running more or less in an EW direction.

Looking at the geology of the studied region in detail, it can be clearly observed that the fundamental geologic properties of the Marmara region indicated in Figure 2.6 are principally constituted of three parts: the Sakarya zone (Ophiolites and Ganitoids) and Karakaya Complex are clustered as Sakarya zone in Figure 2.6, Istanbul zone and Istranca massif (Ketin, 1973; Okay, 1986). The Istanbul Zone is a little continental fragment, about 400 km long and 70 km wide located in the southwestern margin of the Black Sea (Figure 2.5), has been described by a well-developed, unmetamorphosed and minor deformed continuous Paleozoic sedimentary succession extending from Ordovician to the Carboniferous overlain with a major unconformity by latest Permian to lowermost Triassic continental red beds (Okay, 1986). The Istanbul zone is certainly distinct from the tectonic components located in the surrounding area due to its stratigraphy, the nonexistence of metamorphism and lack of major deformation (Okay, 1986). The Sakarya zone is defined by a variably metamorphosed and seriously deformed Triassic basement called the Karakaya Complex (Figure 2.6) overlain with a major unconformity by Liassic conglomerates and sandstones which passes up to Middle Jurassic-Lower Cretaceous limestones and Upper Cretaceous flysch (Okay, 1986). In contrast to the Istanbul zone, the Sakarya zone does not have a Paleozoic basement.

The Izmit Gulf is an east-west trending dynamic graben system. It is dynamically influenced by the interplay between the NAF and the Marmara Graben system (Onder Çetin et al., 2004). The graben is enclosed by two horsts: the Kocaeli Peninsula to the north and the Armutlu Peninsula to the south, indicating quite distinct geomorphological features, and by well-defined fault scarps (e.g., Onder Çetin et al., 2004) (see Figure 2.5) and 2.6). The Armutlu Peninsula and the surrounding areas within northwest Anatolia include three geologically distinct zones: southern, central and northern. The southern zone corresponds to the Sakarya Continent and substantially includes thick Mesozoic sedimentary sequences (Yılmaz et al., 1995). The center zone basically comprises of the Iznik metamorphic accumulation and Geyve metaophiolite. The northern zone is known as the Armutlu metamorphic accumulation and fundamentally comprises of indistinctly-metamorphosed rocks, evaluated as the Rhodope-Pontide basement (Yılmaz et al., 1995).

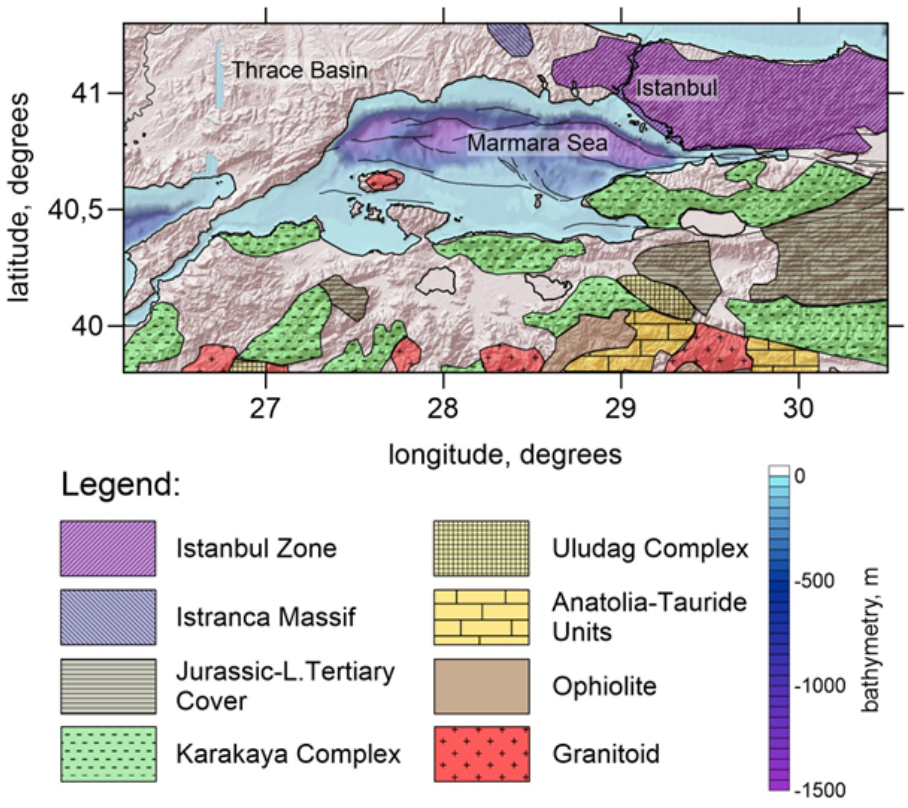

Figure 2.6. The main geological components of the Marmara region (modified by Okay (1986) after Ketin (1967)).

In addition to the Gulf of Izmit, another important gulf is the Gemlik Gulf which is located along the Middle strand of the NAF (Figure 2.5). Although GPS data (e.g., McClusky et al., 2000; Meade et al., 2002; Straub et al., 1997) show that slip rates at the Middle NAF strand are much lower (few mm/yr) than those at the northern branch, morphological and bathymetric data clearly indicate that this region is quite active and has a diffuse set of faults and fractures visible at the seafloor and controls the formation of the Gemlik Bay depression (Gasperini et al., 2011).

2.2. Geophysical Background

As mentioned in section 2.1, the geologic structure of the study region is very complex. Several geological and geophysical studies (e.g., Barış et al., 2005; Honkura et al., 2000; Koulakov et al., 2010; Okay et al., 2000) have been carried out to understand tectonic evolution and geologic structure of this area. For instance, a 3D local tomography technique was applied to travel time data derived earthquakes from 1985 to 2002 occurred in the Marmara region by Barış et al. (2005). As a result of this study, they observed strong lateral heterogeneity in this area.

Another significant research of this region was carried out by Koulakov et al. (2010). Low speeds underneath the primary sedimentary basins (e.g., Adapazarı, Düzce, and Kuzuluk are indicated in Figure 2.5) were observed in this study. In addition to this, high-velocity and low attenuation patterns were observed in the study. The findings well corresponded with blocks assumed to be solid (Almacık, Kocaeli and Armutlu blocks are indicated in Figure 2.5 and 2.6).

Furthermore, the combined analysis of magnetic and gravity fields, electrical and magnetotelluric measurements (e.g., Honkura and Işıkara, 1991; Honkura et al., 1985, 2000) have uncovered obvious anomalous zones associated with the uncertainty of the extent of fracturing in diverse branches of the NAF. Similar features were also found by the analysis of the consequences of the joint modeling of gravity and reflection seismic data gathered in the Sea of Marmara (Adatepe et al., 2002).

Different research groups (e.g., Gürbüz et al., 2000; Nakamura et al., 2002; Salah et al., 2007) investigated in the crustal seismic structure of the western part of the NAF by using tomographic methods. 2-D tomographic seismic velocity image (Karabulut et al., 2003) is another study which revealed that in the eastern Marmara region along a N-S trending seismic refraction profile traverses Çınarcık Basin in the Sea of Marmara (see Figure 2.5). Plenty of the researches were based on the inversion of P- and S-wave travel-time arrivals from local seismicity recorded by stations belonging to temporary and /or permanent networks.

In a study carried out by Tunc (2008), the three-dimensional velocity structure of the Marmara Region was investigated by tomographic inversion method. For this study, LOTOS-07 algorithm developed by Koulakov et al. (2007) was used. This study shows that the three-dimensional structure of the crust under the Marmara Region down to 15 km depth is in good resolution. Further, it was observed that the findings from the study are coherent with previous gravity, magnetic and electromagnetic profiling studies for the region and as well as previous tomographic images obtained by other researchers (e.g., Gürbüz et al., 2000; Nakamura et al., 2002; Karabulut et al., 2003; Salah et al., 2007).

Other important projects consisting of A Multi-Channel Marine Seismic and 2-D Wide Angle Reflection Refraction were done (Bécel et al., 2009; Laigle et al., 2008) in this region. In particular, the profiles of the projects present only information about the depth variations of the basement of up to 7 km between the North Marmara Through (NMT) and its surroundings. Bayrakcı et al. (2013) used the first 16000 arrival times of artificial sources and inverted them with the well-known local earthquake tomography (LET) code Simulps (Thurber, 1983) to reveal the 3D upper-crustal heterogeneity of the NMT. Although these studies cover a similar area, their findings indicate substantial incoherences. For the first time, crustal anisotropy underneath the whole Marmara region was investigated by utilizing shear wave splitting method (see Polat et al., 2012). In that study, the 2006 Mb=5.3 Manyas-Kus Golu (Manyas) earthquake has been retrospectively "stress forecasted" using variations in time-delays of seismic shear wave splitting to appraise the time and magnitude at which stress-modified micro-

cracking reaches fracture criticality within the stressed volume where strain is released. The method is very convenient for characterizing variations in tension before and after the impending earthquake, however, it is not enough to reveal changes in the velocity structure of the investigated region.

In Ph.D. thesis study, Çaka (2012) analyzed crustal anisotropy developed in Armutlu Peninsula and surrounding area placed eastern Marmara Sea in between two strands of North Anatolian Fault (NAF) utilizing direct observation, aspect ratio, cross-correlation, and particle motion diagrams methods. Results from the study indicated that stations located around geothermal sources have different polarizations, but dominant polarizations from the other stations seem parallel to the maximum stress direction of the study area. Scattered polarizations in stations near geothermal sources interpreted as an effect of the high-pressure underground water in shallow depth of the area.

Finally, it can be said that although many studies for understanding the district have been performed, the detailed crustal structure of the study region, especially the southern part of Marmara region, is unknown in detail. In our study, we aim to construct the new crustal model of the entirety of the Marmara region by utilizing a new strong dataset. We will thus produce new information about the whole region based on knowledge obtained from the local tomography and shear wave splitting analyses.

Considering destructive earthquakes (the 17 August 1999 Kocaeli earthquake (Mw=7.4) and the 12 November 1999 Düzce earthquake (Mw=7.2)) in the Marmara region, it is clearly noticed that the historical and recent seismicity of the Marmara region is plenty high. This heavy seismically activity enables us to collect strong datasets. At the same time, this high rate of seismicity is of a vital significance for the earthquake risk in the Marmara region because of a majority of Turkey's population and a large number of industrial centers located there. For this reason, such a study is significant to acquire mighty and trustworthy information with regarding the crustal structure of the investigated region.

3. DATA

In chapter 3, information about instruments and collected data is given. Relocation processing of the collected data is also presented. The chapter is completed with detailed information about the quality of data discussed.

3.1. Seismometers

For this study, data from broadband and short-period stations (Figure 3.1) installed by Bogazici University, Kandilli Observatory and Earthquake Research Institute (KOERI) and the Scientific and Technological Research Council of Turkey (TUBITAK) during the Multi-Disciplinary Earthquake Research in High Risk Regions of Turkey project (TURDEP) in the Marmara Sea region were gathered.

The short period and broadband seismic stations must have three components. 5 OBS stations were also used (Figure 3.1). All seismometers from KOERI acquired continuous data between 2005 and 2011. The on-line broadband stations of the TURDEP project were also used. There are a few stations of Prime Ministry Disaster and Emergency Management Authority, Republic of Turkey (AFAD) utilized in this work. The majority of the utilized receivers are permanent. The OBSs from KOERI recorded seismic events between the dates of 2006 and 2011. During this study, we additionally added some permanent KOERI stations (Figure 3.3) to our fundamental stations (Figure 3.1) to improve data quality and ray coverage locally. Some of the stations were deployed in this area between 38^0-39^0N and 26^0 -30^0E. Others were installed between 39^0-41^0N and 32^0 -33^0E.

3.2. Relocation of Collected Data

Firstly, all events within the time period of 2005-2011 based on the event catalog of the Boğaziçi University Kandilli Observatory and Earthquake Research Institute (KOERI) was mapped before the relocation analysis (Figure 3.2).

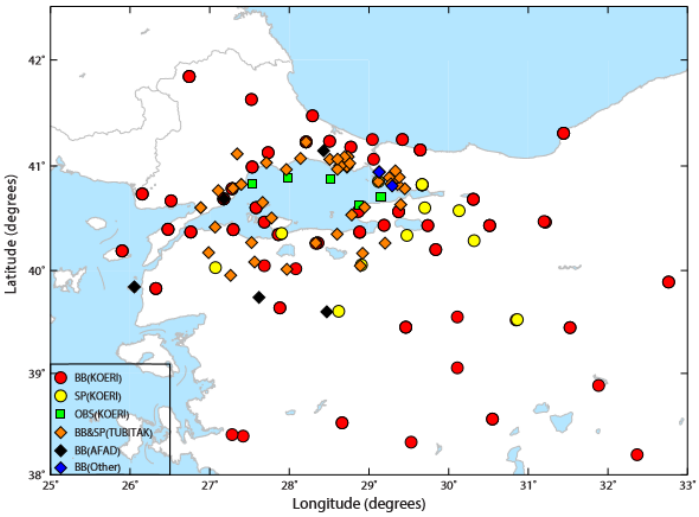

Figure 3.1. The majority of seismic stations of the study consist of Broadband (BB), Short Period (SP) and Ocean Bottom Seismic (OBS) stations of KOERI illustrated by red, yellow circles, and green squares, respectively. BB and SP stations of the TUBITAK are indicated as orange diamonds. BB stations of the Prime Ministry Disaster and Emergency Management Authority, Republic of Turkey (AFAD) and BB stations of other institutions are indicated as black and light blue diamonds, respectively.

Then, more than 60 percent of all the events were discarded from the data set due to the local magnitude less than 2. After that, nearly 4000 seismic events with magnitudes ML≥2 occurring from 2005 to 2011 in our study region between 39^0–42^0N and 25.6^0 –32^0E geographical coordinates were relocated by using zSacWin (Yılmazer, 2003). The processed events are classified in terms of depth and magnitude (Figures 3.3 and 3.4). The used software for the seismic event processing is based on HYPO71 (Lee and Lahr, 1975). When the relocation procedure was applied to the earthquakes, the quality of the recorded three-component waveforms was visually checked. During this analysis, more than 800 earthquakes were removed from the dataset due to lack of high quality. We have given particular attention to obtain a good signal to noise ratio of the incoming wave and to detect obviously P and S phases on the waveforms associated with the seismic events. Additionally, we applied a Butterworth filter with a 2-16 Hz band range utilizing a two-way 4-pole on the seismograms in order to suppress

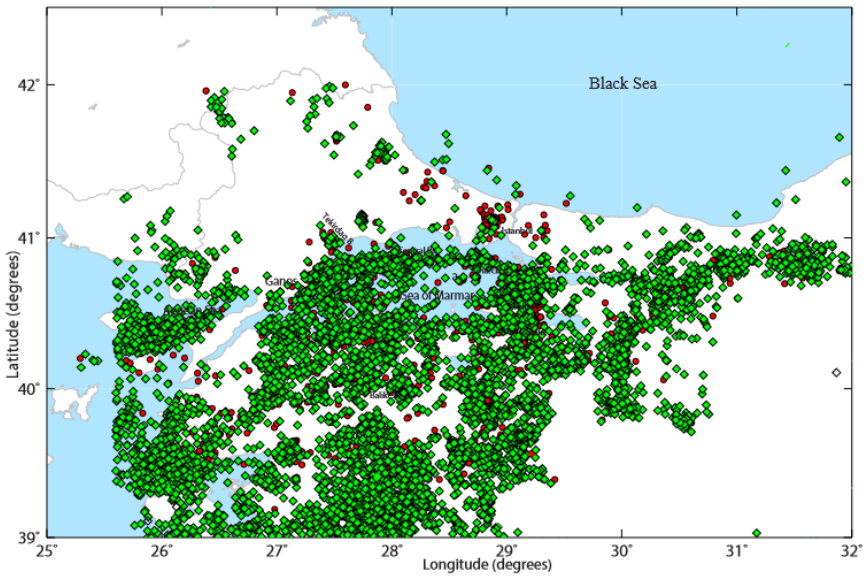

Figure 3.2. Green diamonds and red circles show the dissemination of earthquakes before and after the relocation, respectively.

the high-frequency noise and detect precisely P and S phases on each seismogram. It is valuable to mention here that arrival times for P and S phases were certainly controlled by visual inspection.

If P and S wave arrivals of the seismograms are certainly visible, the phases were manually picked. Noisy and highly attenuated S wave recordings caused by the high attenuation of the study area were observed by some earth scientists (e.g., Bindi et al., 2006; Horasan et al., 1998). In order to get rid of distorted recordings, waveforms were merely analyzed by eye. In this way, exclusively the high-quality probable recordings for further analysis were selected. For relocations, P- and S-wave readings were utilized and the magnitudes were generally calculated by applying a duration dependent formula generally utilized for local seismic events at the KOERI. For small and local seismic events, the duration dependent formula is helpful (Barış et al., 2005). During the relocation analysis, as weights for P and S waves, values of 1.0 and 0.5 were chosen. The value of Vp/Vs 's ratio was assumed as 1.735 for this study. Since this value was usually utilized by KOERI for routine locations of local seismic events that occurred in the western part of Turkey. In advance of the relocation analysis, we observed that the

average horizontal and vertical ambiguities of the gathered earthquakes are more than 4 and 5 km, respectively. Therefore, we cautiously relocated the events to diminish these ambiguities. Furthermore, the dataset was restricted by the following criteria: 1) the standard error of epicenter and depth is less than or equal to 2 km, 2) the number of P phase readings is more than 7, and 3) the rms of arrival time residual is less than 0.9 s. Besides, seismic events with azimuthal gap less than 180^0 and recorded by at least 7 seismic seismometers were merely selected.

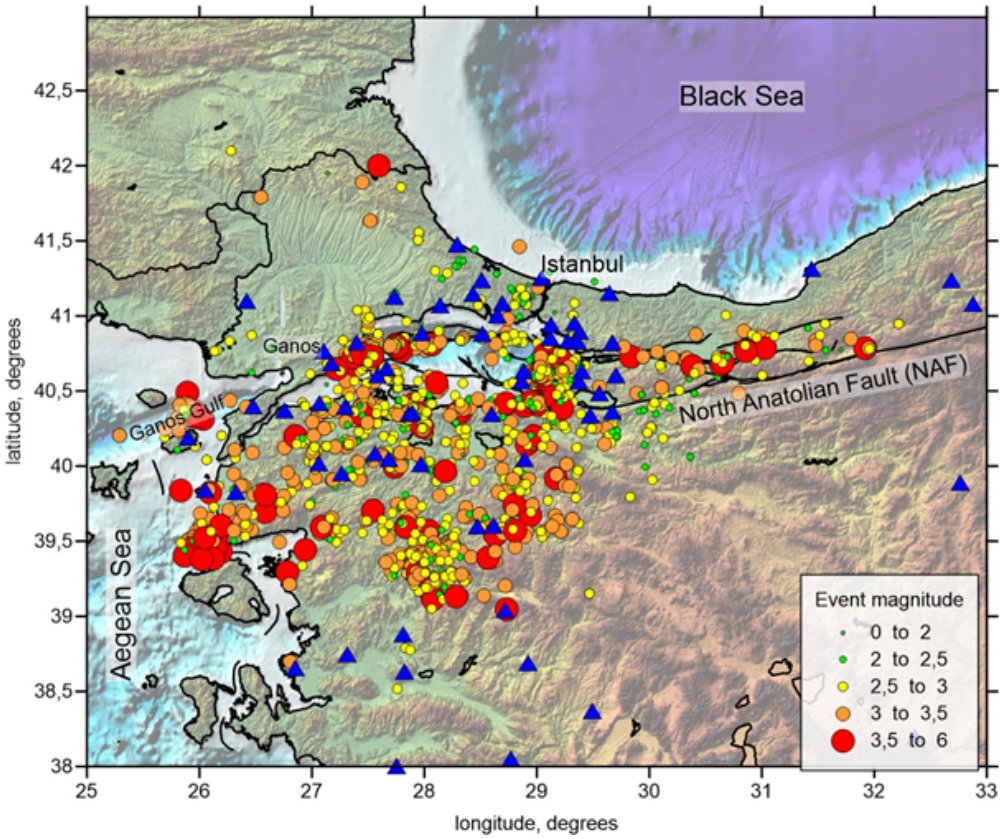

Figure 3.3. The seismic stations and earthquakes used in the study were marked with triangles and circles, respectively. The magnitudes of the seismic events were denoted with the colored symbols.

The final earthquake catalog comprised of local moderate and particularly microearthquakes with magnitudes ML≥2. In general, microearthquakes are related to the NAF segmentation in the Sea of Marmara, whereas the seismic events with magnitude Mb ≥5.0 are along the NAF in the Marmara region (Figure 3.4). As seen in Figure 3.4, the recognized seismicity in the Sea of Marmara is fairly consistent with

the common fault geometry located in the sea.

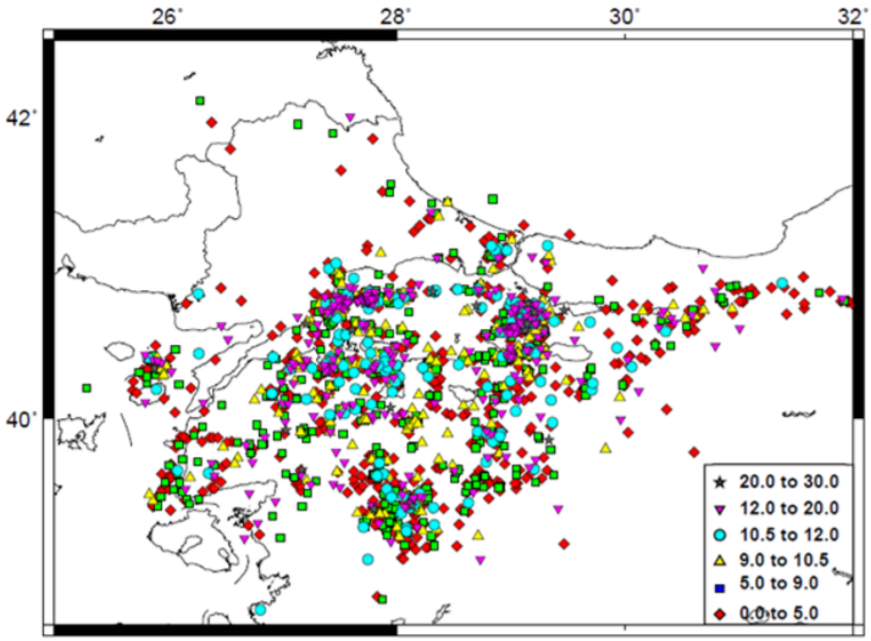

Figure 3.4. The used seismic stations and the selected earthquakes in this study were marked with triangles and circles, respectively. The used events are color-coded in accordance with the focal depth

But, it is not observed any similar compatibility between the seismic events happened in the Central and Cınarcık basins. It is clearly observed that the seismic activity of the investigated region concentrates at the left and right boundaries of the northern branch of the NAF in the Sea of Marmara.

In this catalog, the greatest event is the 2006 Manyas EQ with magnitude Mb= 5.3. After the happening of the seismic event, no earthquake greater than magnitude 5.0 has been recorded in the Sea of Marmara during the 5-year-period of the study.

A few earthquakes occurred in the southern part of the study region, are artificial blasts, are related to mining work. But, here the events were not utilized as active sources because of the lack of their origin times and coordinates in the catalog. Therefore, in the relocation procedure, the events were processed as passive sources in

the same way as earthquakes. Later, such the artificial blasts were removed from the catalog because of no available or too weak S waves.

4. LOCAL TOMOGRAPHY

A local tomography method is described and the results of local tomography obtained from this study are presented in this chapter.

4.1. Local Tomography Method

During this study, the selected events were successfully analyzed by using a local earthquake tomography (LET) method. For the tomographic inversion analysis, the LOTOS code (Koulakov, 2009) was used. This code has been successfully implemented to different datasets by many earth scientists such as Bianchi et al. (2013).

A general structure of the main steps of this code is shown in Figure 4.1. The detailed inversion structure for the code is presented in Figure 4.2. The Vp-Vp/Vs inversion scheme has the same structure of programs, however only for node parameterization (see Koulakov (2009) for detail information about the code). In this analysis, the coordinates of receivers and arrival times of P and S rays from local events to these receivers are given as input data. As seen in Figure 4.1, a starting velocity for 1D and or 3D, parameters for location, grid construction, inversion, and others can be defined by the user as additional information.

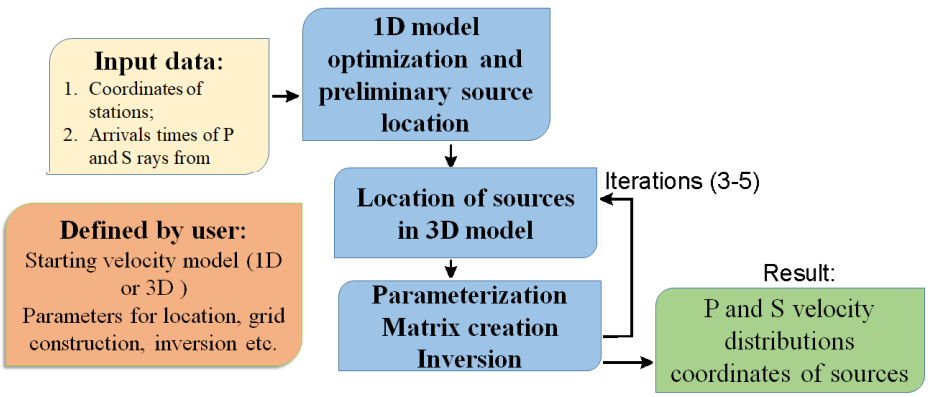

Figure 4.1. The general structure of the LOTOS code. Taken from Koulakov (2009).

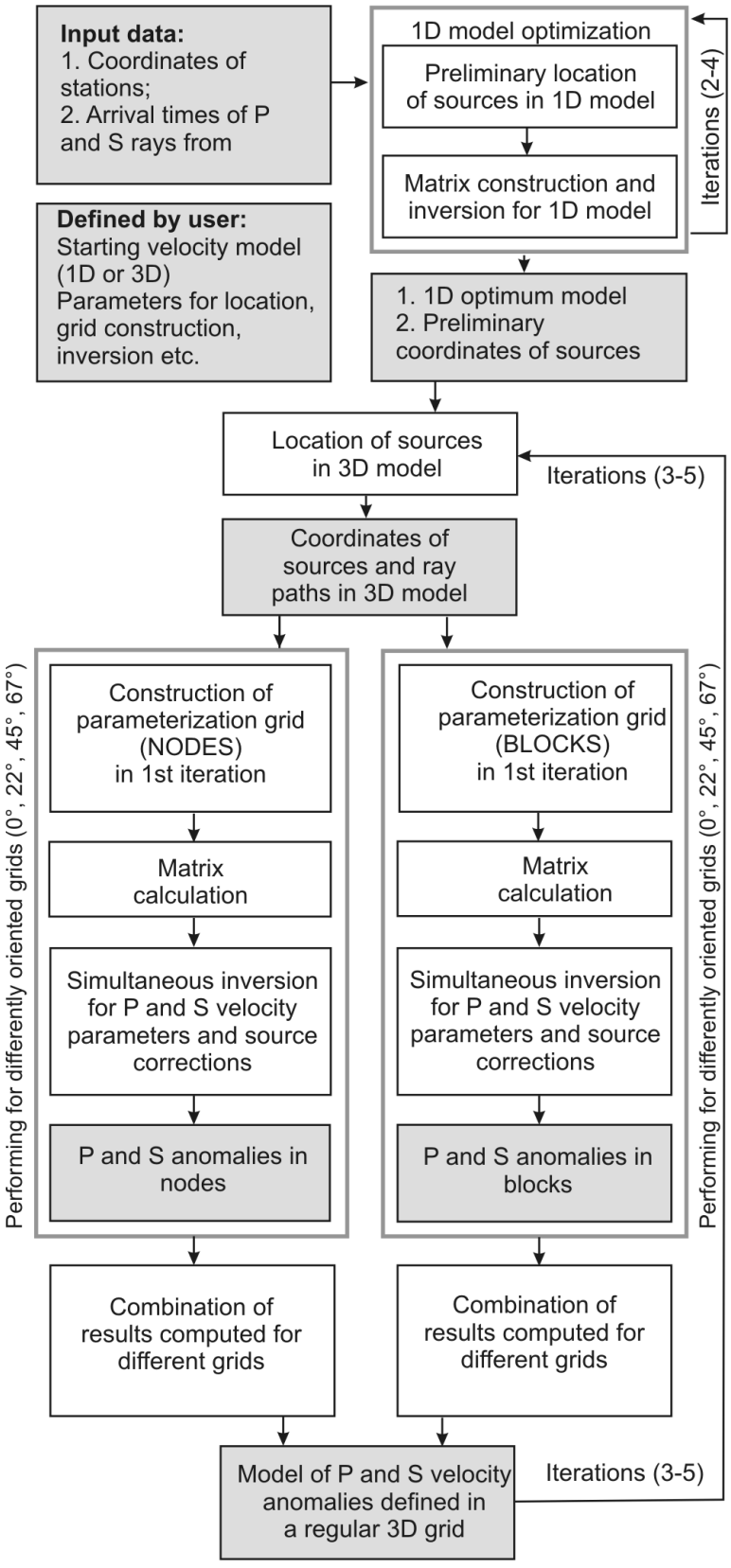

Figure 4.2. The detailed structure of the LOTOS algorithm. Taken from Koulakov (2009).

Preliminary locations and origin times of earthquakes can be provided by picking tools and/or catalogs, but it is not necessary for the local tomography analysis because the code starts searching for the source hypocenter either from the center of the network or from the station with minimal arrival times (Koulakov, 2009). One of the important features of the code is that the procedure starts with the relocation of all earthquakes utilizing the grid search method. The algorithm of the code is based on the following steps: 1. Simultaneous optimization for the best 1D velocity model and a preliminary location of sources; 2. Location of sources in the 3D velocity model; 3. Simultaneous inversion for the source parameters and velocity model utilizing many parameterization grids.

During the analysis, steps 2 and 3 were iterated in turn one after another in many iterations.

4.1.1. Algorithm for 1D Velocity Optimization and Preliminary Source Location

The code algorithm for 1D velocity optimization and preliminary source location is presented in Figure 4.3

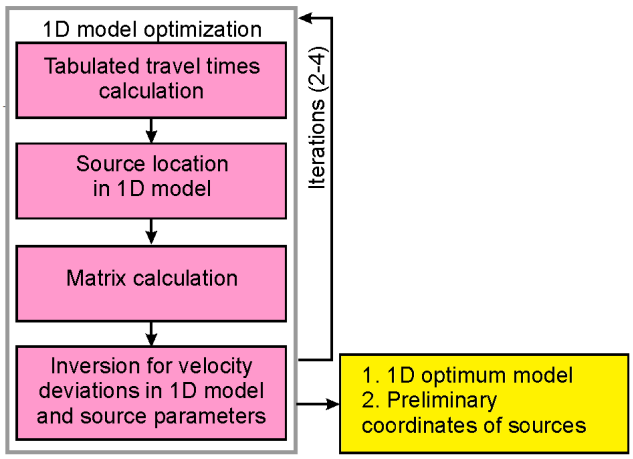

Figure 4.3. The main steps for the 1D velocity optimization and preliminary source locations. Taken from Koulakov (2009).

4.2. Data

For the application of the tomographic inversion, 2131 events were chosen with regarding two criteria: (1) the number of phase readings of both P and S data is more than 15 in total, and (2) the deviation of residuals after 1D velocity inversion step is less than 1 s. As a result of this, 50044 P and 42814 S travel time data were acquired. The chosen earthquakes are illustrated in Figure 3.4. In this study, the LET method has been successfully implemented to the chosen seismic events. For the tomographic inversion procedure, we utilized the LOTOS code (Koulakov, 2009). As mentioned steps before have been properly followed during the processing. We initially started the procedure with the relocation of all earthquakes utilizing the grid search method.

Travel times from the dataset at this stage were calculated utilizing a reference table computed prior to the relocation step. The earthquake sources were relocated utilizing the 3D algorithm of ray tracing. The first iteration utilizes a starting 1D model. However, in the next iterations, the relocation analysis is implemented utilizing the updated 3D velocity models. During this procedure, the ray tracing was implemented based on the bending method.

The beginning 1D velocity model was described in many depth levels with utilizing linear interpolation between levels. The upper level of the 1D model was described at the altitude above the maximum elevation taking place in the study area. For the 3D tomography inversion, the optimal 1D starting model was determined after many runs of the full inversion procedure consisting of inversions and earthquake source locations in many iterations.

As first, we start with an approximate 1D model restricted from available in advance of information. After full inversion, we compute average absolute velocities at a few depth levels and use these values as a starting 1D model for the next run. After three or four runs, the velocities converge to stable values and the procedure stops. Table 4.1 presents the resulting P and S velocities utilized as a reference model for the ultimate results. At shallower depths, we observed higher velocities than generally

expected in continental areas. The parameterization of the velocity dissemination was performed utilizing a mesh of nodes distributed in the study area according to the data dissemination. In this study, the minimum grid spacing for the horizontal and the vertical directions are 7 and 3 km, respectively.

Table 4.1. P- and S- wave speeds in the 1D model utilized for calculations of the primary results of this study.

Depth, km	Vp, km/s	Vs, km/s
-1	5.63	3.19
5	6.03	3.46
10	6.21	3.53
15	6.36	3.62
20	6.61	3.77
30	7.31	4.21

We have utilized ∼18,000 and 16,000 nodes, which compose one grid for the P and one grid for the S model, respectively. The grid spacing is explicitly described to be smaller than the minimum size of resolved anomalies so that every robust pattern in the resulting model contain many nodes.

In this situation, the resolution becomes grid independent: modifying the mesh (i.e., shifting or rotating the grid) does not influence the solution. But, to further reduce artefacts related to the main grid orientation, independent inversions for four grids with distinct fundamental orientations (0^0, 22^0, 45^0, and 67^0) were performed.

The inversion was implemented simultaneously for the P- and S-velocity anomalies, as well as for the source parameters (3 coordinates and origin time for each event) and receiver corrections. The quality of the resolution was examined by extra matrix blocks, which arrange velocity gradients between neighbouring nodes. This arrangement connected the velocity parameters in all pairs of neighbouring nodes and perform the parameterization quasi-continuous. In this situation, the solution was checked by the flattening coefficients, and not by characteristics of the grid. The values of damping parameters and weights for various groups of parameters are experimentally described

based on the results obtained from various tests. In particular, the correct smoothing coefficient should not allow for the appearance of small contrasted patterns, which cannot be resolved by synthetic tests and not similarly observed in the odd/even test.

The sparse matrix is inverted using the least-squares QR method (der Sluis and van der Vorst, 1987; Paige and Saunders, 1982). After inversions in four differently oriented grids, the results were averaged and recalculated in a regular grid. This model is utilized as reference dissemination for the next iteration which starts with the relocation of sources. The tomography cycle, which is repeated several times, includes the steps of source locations in the updated 3D model, matrix calculation and inversion. The effect of iterating and damping is similar: many iterations with strong damping yield a similar solution as with a few iterations and weak damping. Thus, we had preferred fixing the number of iterations at five as a reconciliation between the accuracy and calculation speed and selecting damping coefficients to find an appropriate solution.

After five iterations, the rms values of the P and S arrival time residuals and their reductions were acquired as listed in Table 4.2. The residuals of the first iteration correspond to the location in the formed1D model. Other iteration values in Table 4.2 show how the 3D velocity inversion leads to an improved data fit. The values of the residuals obtained from the dataset are fairly different initially (0.238 and 0.419 s for P and S data, respectively) when compared to those for a dataset collected in the eastern Marmara region. For instance, for the eastern Marmara region (Koulakov et al., 2010) in the first iteration, the rms of P and S residuals were 0.137 and 0.255 s. It is significant to note that the same algorithm was utilized for data processing both in the present and the mentioned study. It might suggest that for a prior indicator of the amplitude of the velocity anomalies, it may be probable to utilize the rms of the initial residuals.

The average deviations of residuals in the L1 norm during iterative inversions are also listed in Table 4.2. It may be observed that the inversion ensures the reduction of residual deviations by nearly 30% for P- and 47.5% for the S-wave data. The final

average deviations seem to be compatible with estimates of the picking accuracy (0.15 and 0.20 sec for P and S phases, respectively). Larger reduction of residuals for the S data might be related to the higher sensitivity of the S data to variations of physical parameters inside the Earth.

Table 4.2. Average deviations of the P- and S-wave residuals and the variance reductions after five iterations of inversion. ∗rms dtp and rms dts stand for the P- and S-wave residuals, respectively.

Iteration	rms dtp∗ (sec)	rms dts∗ (sec)	Reduction P(%)	Reduction S(%)
1	0.238	0.419	0	0
2	0.183	0.250	22.84	40.41
3	0.172	0.230	27.50	45.18
4	0.167	0.222	29.57	46.89
5	0.166	0.220	30.20	47.46

4.3. Tomography Results and Testing

P- and S-velocity anomalies in four horizontal slices at 5, 15, and 30 km depth were indicated in Figure 4.4. The P- and S-velocity anomalies were additionally shown for one vertical section in Figure 4.5. At shallow depths, their amplitudes were less than 5%, whereas, at a depth of 30 km, they are less than 2%. During the application of the inversion, the amplitude damping was reduced and the smoothing damping at a minimal value providing stable results was also described.

The values of the inversion parameters were established with regarding the results of synthetic modeling enabling the maximum similarity between the initial and recovered models, both in terms of amplitude and the positions of the synthetic patterns.

In advance of evaluating these findings, a few tests to evaluate the resolution and the reliability of the derived structures were performed. The results of several checkerboard tests were shown in Figure 4.6. Here we indicated the reconstruction outcomes for the whole of models with the anomaly sizes of 20 and 30 km and the amplitudes of ±5%.

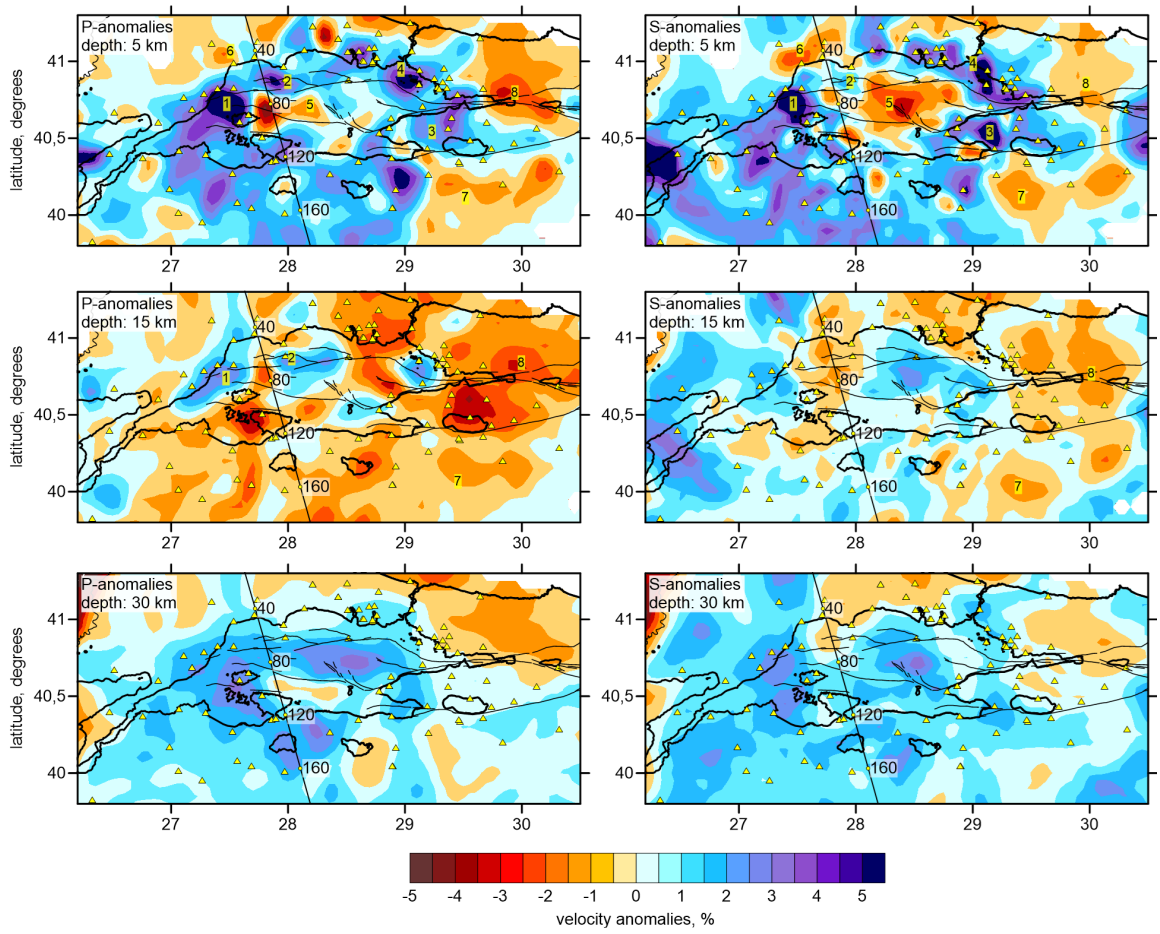

Figure 4.4. P- and S-velocity anomalies in four horizontal sections. Seismometers are marked with triangles. Important faults in the Marmara Sea (same as in Figure 3.1), were exhibited with thin lines. The black line shows one vertical section that was chosen for showing the P- and S-velocity anomalies in Figure 4.5.

Travel times for the synthetic tests were calculated utilizing 3D bending ray tracing based on the identical source-station pairs as in the real dataset. Then, they were perturbed by random noise with an rms of 0.1 s for P and S-wave data, respectively. The reconstruction workflow and parameters were definitely the same to those implemented for the analysis of experimental data consisting of the step of the initial source location.

Figure 4.6 indicated merely results for the P-velocity reconstructions; for the S

model, the reconstruction quality was like and even better. It may be seen that in shallow depths (left column), all models were properly reconstructed in most parts of the area. The sections in the right column indicated the deepest sections where the comfortable recovering of synthetic anomalies were reached. It can be observed that the anomalies of 20 km size were strongly reconstructed down to 15 km depth;

The sections in the right column represent the deepest sections where the satisfactory recovering of synthetic anomalies is achieved. It can be seen that the anomalies of 20 km size are robustly reconstructed down to 15 km depth; 30 km anomalies were observable down to 30 km depth, while the 50 km anomalies were restored in all depth intervals. Based on these tests, it may be concluded that the ray configuration theoretically allows for reconstructing the shapes of small patterns at only shallow depths, whereas the large anomalies of more than 50 km size are strongly recovered at all depths. Note however that the amplitude of the reconstructed anomalies decreases with depth. These observations should be considered when assessing the results of experimental data inversion.

A much more significant test with independent inversions of two independent data subsets, the so-called, odd/even test, as shown in Figure 4.7. In this situation, the whole dataset was divided into two subsets with odd and even numbers of earthquakes. The difference between the extracted results reflects the effect of random noise. For the P-model, the locations of the primary anomalies are similar in both cases; however, their shapes and amplitudes in some parts of the Marmara region were fairly distinct. For the S-wave velocity anomalies, the comparatively strong characteristics were resolved in shallow depths. For the deeper section, the anomalies extracted from the odd and even subsets do not match that show a significant role of the random factor. Therefore, the corresponding results should be commentated with prudence.

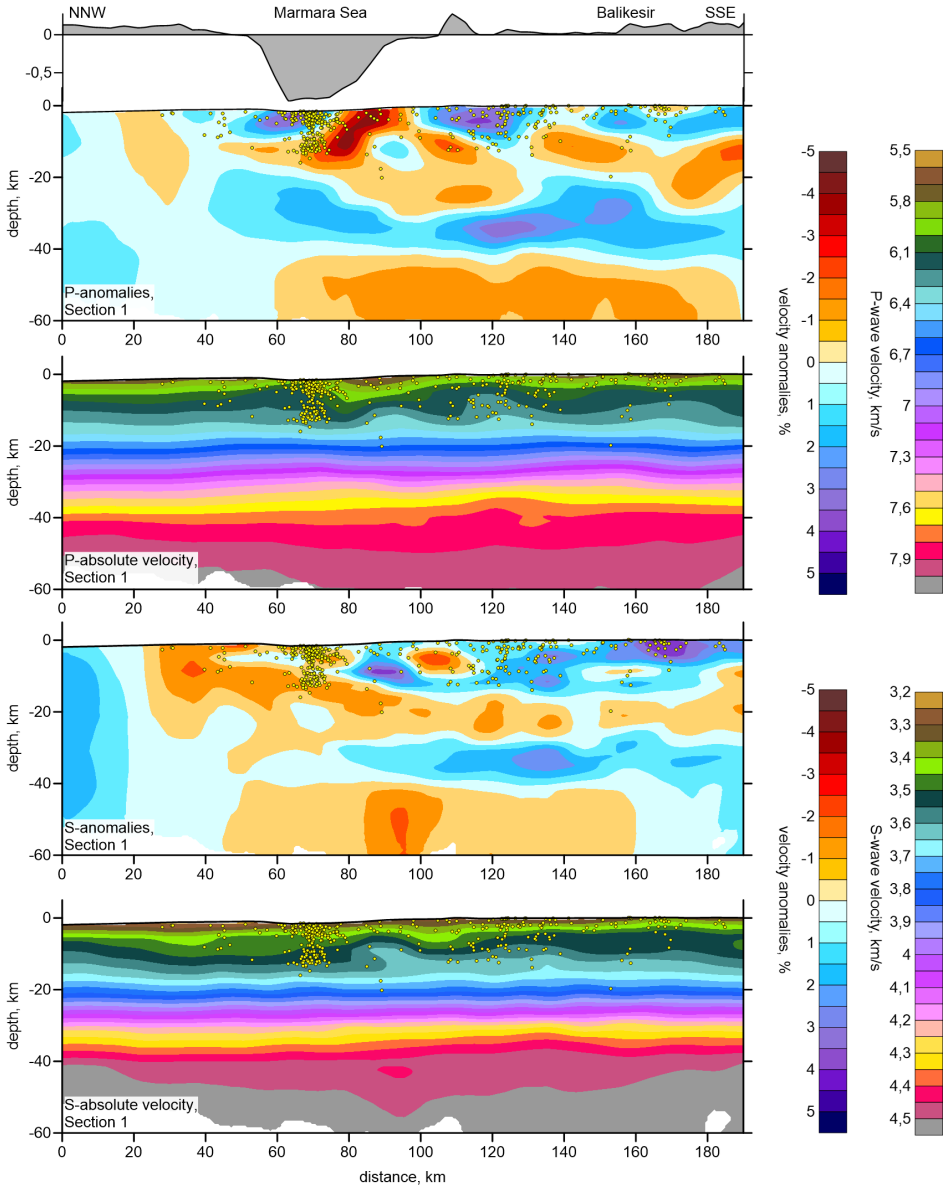

Figure 4.5. Perturbations and absolute values of the P- and S-wave velocities in a vertical section. Location of the profile was indicated in Figure 4.4. The dots illustrated the earthquakes located at distances smaller than 15 km from the profile. The topography along the profile was exhibited in the upper part of the figure. Note that the upper surface in the velocity sections takes into account the earth′s sphericity.

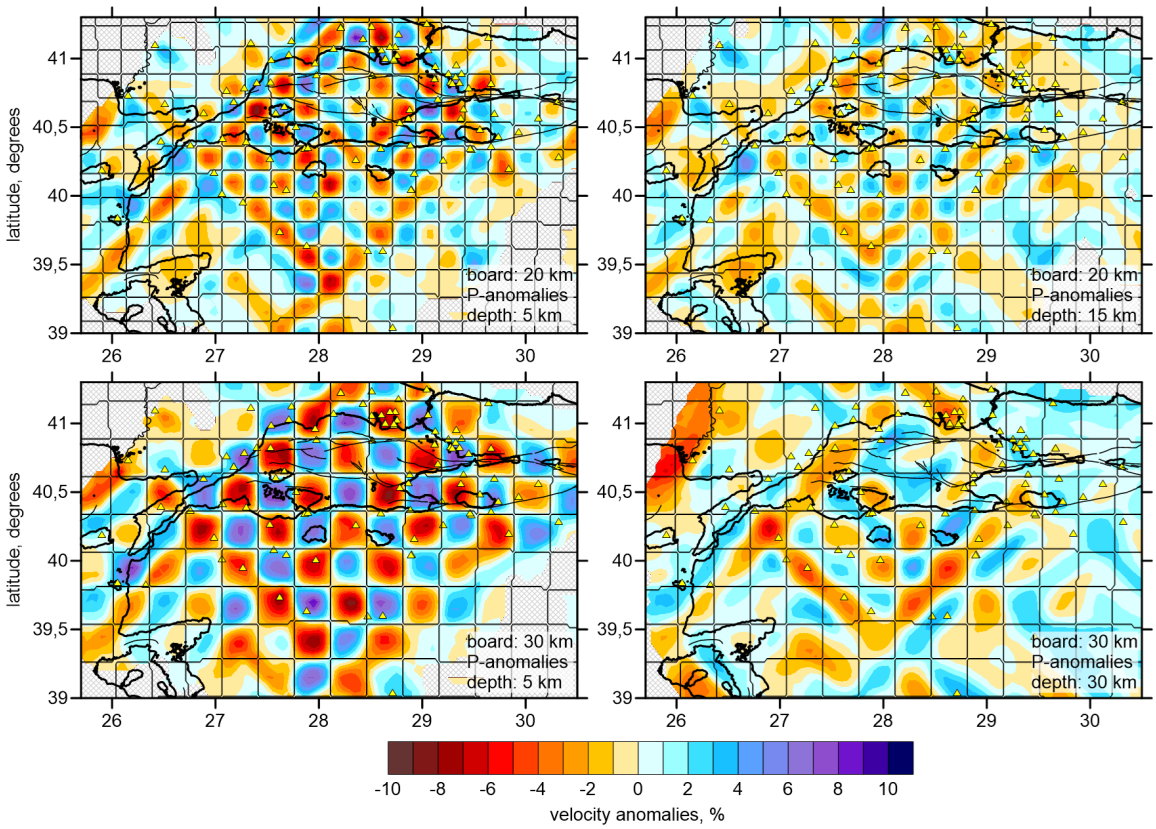

Figure 4.6. Reconstructions of three checkerboard tests with anomaly spacing of 20 and 30 km. The shallower section is at a depth of 5 km and the deeper sections are at distinct depths corresponding to the deepest level where the recovering is satisfactory. Shapes of anomalies were shown with thin line contours. Triangles indicated seismometers.

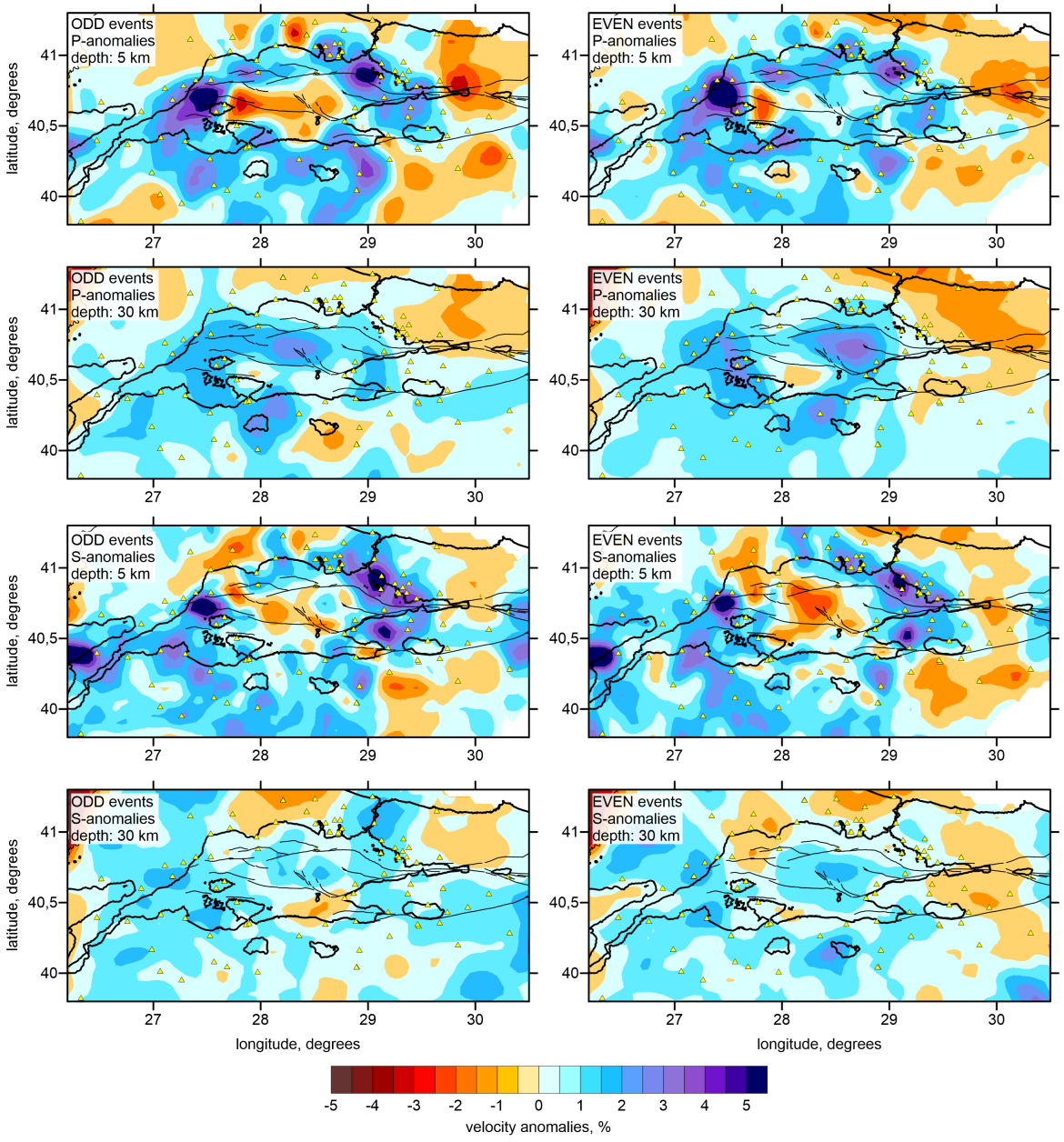

Figure 4.7. Odd/Even test. Left and right columns are the reconstruction results for independent data subsets with odd and even numbers of earthquakes, respectively. Triangles indicated receivers. Significant faults in the Marmara Sea (same as in Figure 2.5), were shown with thin lines.

5. SHEAR WAVE SPLITTING ANALYSIS

Theoretical and applied studies of seismic anisotropy indicated that the concentration of tension before seismic activities may be monitored by determining variations in the time delays between split shear waves along a certain range of ray-path directions in the shear-wave window (Crampin and Zatsepin, 1997; Gao and Crampin, 2004; Volti and Crampin, 2003a, b). The study carried out by Crampin et al. (2008) demonstrated that tension-induced variations in microcrack geometry cause variations in shear-wave splitting.

This study is a good example to get information temporal changes in shear-wave time-delays observed in retrospect in advance of a seismic event. In general, the mentioned term stress-forecasting is utilized rather than stress the different formalism. Due to present studies, it can be said that current techniques have been insufficient to exactly detect time and emplacement of earthquakes. But, it is possible to improve in reliability and skill of the present methods relating to probabilistic earthquake forecasting. If these improvements in the methods would be done, time-dependent hazard information potentially useful in reducing earthquake losses and enhancing community preparedness and resilience can be provided (Jordan et al., 2011). In the study carried out by Crampin (1999), it is obviously observed that when variations were recognized soon sufficient, the time, magnitude, and fault break of an M=5 earthquake in southwest Iceland were successfully stress forecasted in a narrow time-magnitude window. To clarify the correlation between changes in splitting parameters and low-level (pre-fracturing) deformation, one of the most significant models is the anisotropic poro-elasticity (APE) model proposed by Zatsepin and Crampin (1997).

Rock mass deformation is basically used in this model as a basic basis. In addition to this, in this model, the fundamental assumption is that the cracks in the crust are so closely spaced. Further, Crampin (2004) demonstrated that the APE mechanism depends on fluid movement due to flow or diffusion along pressure gradients between neighboring fluid-saturated grain-boundary cracks and low aspect-ratio pores and pore

throats at different orientations to the tension field. Also, it was well observed that the mentioned model was accurately calibrated in two controlled source experiments done by Angerer et al. (2002). In this part of the thesis, it was observed that changes in shear wave splitting results from the stations used in the study fairly are compatible with the APE model. Before the impending earthquake, a sudden decrease in time delays of this station was observed. Although it is easy to measure splitting parameters, it is too hard to clearly interpret them. This problem was clearly described by Crampin et al. (2008). This study indicated that shear-wave splitting is misunderstood and specify 17 common fallacies in interpretation that disturb several recent analyses of shear wave. But, utilizing swarms of micro-seismic events as the source of shear-waves, 14 characteristics variations in time delays have been observed, retrospectively, before earthquakes worldwide, with one successful stress-forecast in real time (reviewed by Crampin et al. (2008)). During the analysis of shear wave splitting, the mentioned fallacies were taken into account in order to improve the reliability of the splitting parameters. In this study, Mb=5.3 Manyas Earthquake was selected for stress-forecast because its magnitude was convenient to monitor the significative variations in shear-wave splitting.

5.1. Data and Methods

For this study, only microseismic events recorded by two overlapping seismic networks (Figure 5.1) in the Marmara region comprising of a total of 29 stations installed by the TUBITAK during the TURDEP Project and 33 stations deployed by KOERI were used in order to measure splitting parameters. To monitor changes in splitting parameters before and after the main shock called Manyas Earthquake, the three component digital seismograms of microseismic events which occurred from January-2006 to December-2006 (Figure 5.2), were analyzed. A total of 1216 microseismic events, in the study area between 39^0-42^0N and 25.7^0-31.5^0 E geographical coordinates, were firstly selected for the relocation analysis. For this analysis, zSacWin (Yılmazer, 2003.) was used. This software is basically based on HYPO71 (Lee and Lahr, 1975) (Figure 5.2).

The TURDEP data were combined with KOERI data after September-2006. At first, we started analyzing data recorded by KOERI' s stations for the time period between January-September 2006. Then, we added new data collected from the TURDEP project started installing seismic stations of September 2006 to the previous dataset. Before the splitting analysis, arrival times of both P- and S-phases were acquired by visual inspection to improve the quality of the dataset. Those phases were manually picked with a clear S-wave arrival, which was not always apparent due to high attenuation in this region (Horasan et al., 1998; Bindi et al., 2006).

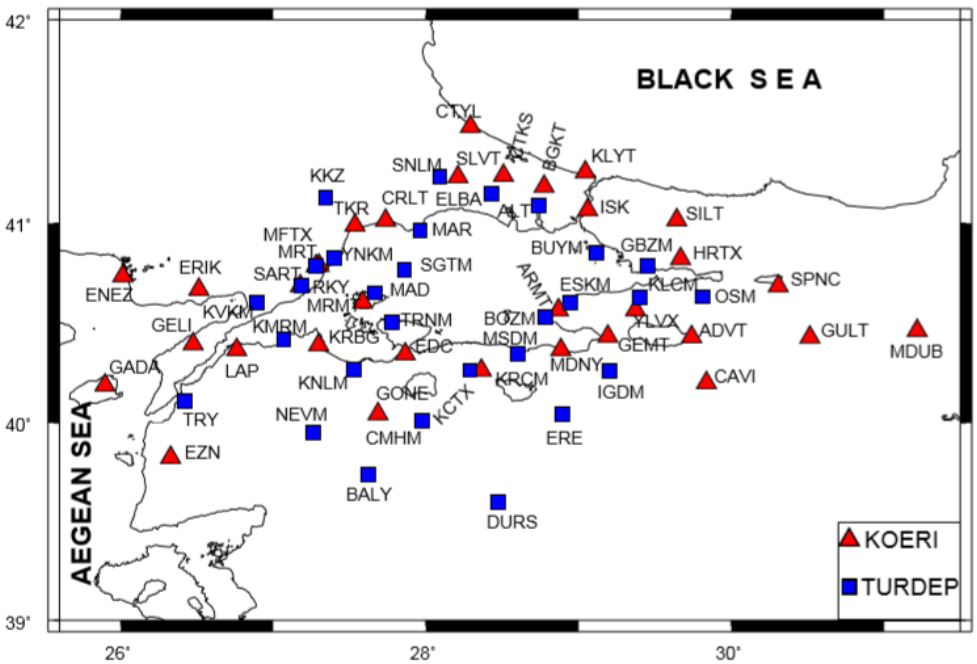

Figure 5.1. KOERI and the TURDEP stations used for this study were represented by red triangles and blue squares, respectively.

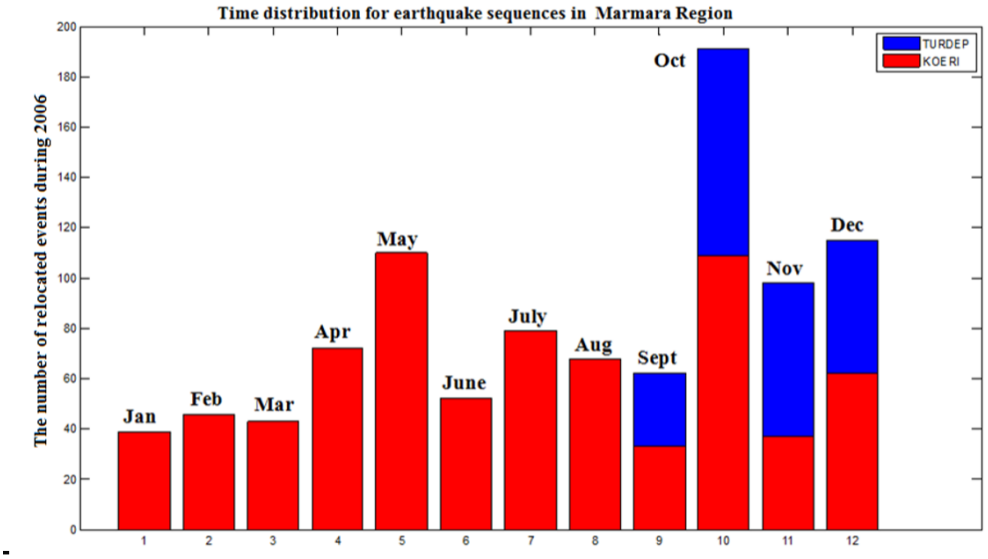

Figure 5.2. The analyzed events by the ZsacWin acquired from KOERI and the TUBITAK stations were depicted with red and blue from January to December 2006, respectively. Here the TURDEP data were combined with the KOERI data for the last 4 months. Also, events occurred in this region starting to be recorded by the TURDEP stations from September 2006.

When location parameters and magnitudes of the earthquakes were calculated, P and S-waves readings were utilized. For small and local seismic events, the duration dependent formula is helpful (Barış et al., 2005). During the relocation analysis, as weights for P and S waves, values of 1.0 and 0.5 were chosen. The value of Vp/Vs' s ratio was assumed as 1.735 for this study (Barış et al., 2005). Since this value was usually preferred by KOERI for routine locations of local seismic events. 1216 microearthquakes were used for the relocation process, however, nearly percentage of 15 of the whole dataset were thrown out from the dataset because of insufficient quality of the events. After the relocation process, some criteria were taken into account to select suitable earthquakes for the shear wave splitting analysis in this study. The considered criteria were listed as follows: (1) the standard error of epicenter and depth is less than or equal to 2 km, (2) the number of phase readings is more than 10, and (3) the rms-value is less than 0.9 s. During this analysis, those listed criteria were definitely considered. After that, the quality of the recorded three component waveforms was

visually checked and those with bad channels were removed. The distance between the recorder and the source should be less than 45 km (Figure 5.2) to obtain the good signal to noise ratio of the incoming wave and detect obviously the impulsive character of the S-wave on the seismogram.

The shear-wave splitting was analyzed on waveforms composed of seismic events that were within the shear-wave window. To get rid of making dirty from S- to P-phase conversions near the surface, the incident angle of a ray path should be less than the critical angle inc= sin−1(Vs/Vp) with Vp and Vs being the near-surface velocities of P- and S-waves, respectively (Booth and Crampin, 1985). For a homogeneous half-space with a Poisson′s ratio of 0.25, the critical angle is inc$\sim 35^0$. Because the low-velocity, near-surface layer outstandingly bends ray paths toward the vertical, a straight line incident angle of 45^0 is adopted as the critical angle in this study (e.g., Shih and Meyer, 1990; Cochran et al., 2003).

The selected seismic events were low-pass filtered from 2 to 16 Hz utilizing a two-way 4-pole Butterworth filter in advance of shear wave splitting analysis. Due to the filter in this range, the high-frequency noise was suppressed. Therefore, the beginning and ending points of the shear wave window for each seismogram were correctly determined. Figure 5.3 indicates a three-component seismogram recorded by station KMR. At the same time, the horizontal components were rotated to get radial and transverse components shown in the figure.

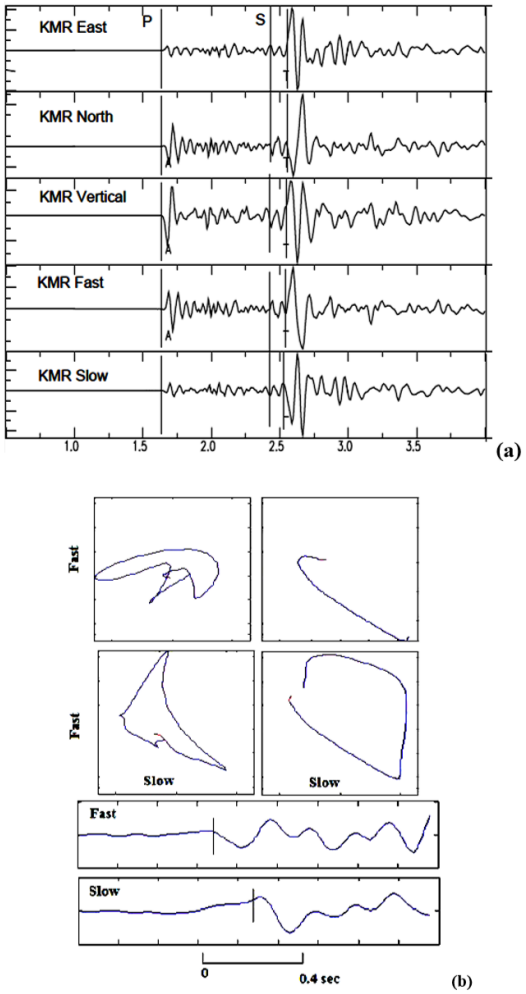

Figure 5.3. (a) A screen image from shear wave splitting analysis before splitting processing. Three component seismogram at a rate of 100 samples per second of a magnitude 2.8 earthquake recorded at station KMR of the TURDEP seismic network in Marmara. The time axis is in seconds. From top to bottom, seismograms are EW-, NS, vertical-, and rotated horizontal components, respectively. P- and S-wave arrivals from the study seismic catalog are also marked on the original seismograms. (b) Screen image of polarisation diagrams for possible adjustment of polarisation and time-delay is exhibited. Fast and slow shear-wave picks are indicated in horizontal polarisation diagrams in time interval 1S and 2S. First and last points of time-delay and directions are detected by visual adjustment.

The magnitude, epicentral distance, and azimuth of the example event shown in Figure 5.3 are 2.8, 5.38 km, and 341^0, respectively. The earthquake was filtered with a low pass-band of 2-16 Hz. Then, two horizontal seismograms of the event were rotated into fast and slow directions where the fast and slow shear-wave arrivals, indicating obvious shear-wave splitting, were shown with vertical lines (Figure 5.3a). The screen image of a polarisation diagram was shown in Figure 5.3. Convenient seismograms were visually chosen for further analysis. Then, the impulsive character of the S wave was visually windowed in terms of an ideal time window. The starting point of the S wave should be started before fast shear-wave arrives and ending the point of the S wave should be ended after the arrival of the slow direct shear-wave. Note that the steps should be done before the scattered coda-waves appear. The high-quality seismogram was windowed with care in order to determine splitting parameters consisting of the delay time δt between the fast and slow direct shear waves and fast polarization direction ϕ. According to Crampin (1999), rises in tension enhance the average time-delay in Band-1 directions of the windowed shear wave at the free-surface, where Band-1 are incident rays making 15^0-to-45^0 to the plane of the parallel micro-cracks. The study carried out by Crampin and Peacock (2008) indicated that the incident shear waves in the remainder of the window, Band-2 directions 0^0-to-15^0 to the crack plane, are sensitive to crack density. In the case of the Band-2, before earthquakes, no variations are observed. Characteristical patterns of rises in shear-wave time-delays in Band-1 directions (Crampin, 1999), showing tension concentration in advance of impending earthquakes, were first recognized in California (Peacock et al., 1988), and later elsewhere (reviewed by Crampin et al. (2008)) consisting of observations on Hainan Island, China (Gao et al., 1998). To reveal variations in tension by utilizing shear wave splitting analysis in advance of the main earthquake, continuous earthquake swarms were chosen in this study (Figure 5.4). Because of the characteristic variation in time-delays of the shear wave, the stress-relaxation reduction was recognized whenever there was enough swarm activity to monitor delays in time. The reduction was assessed as stress pull-off as micro-cracks start to merge onto the fault-plane of the impending seismic event (Crampin and Gao, 2010b).

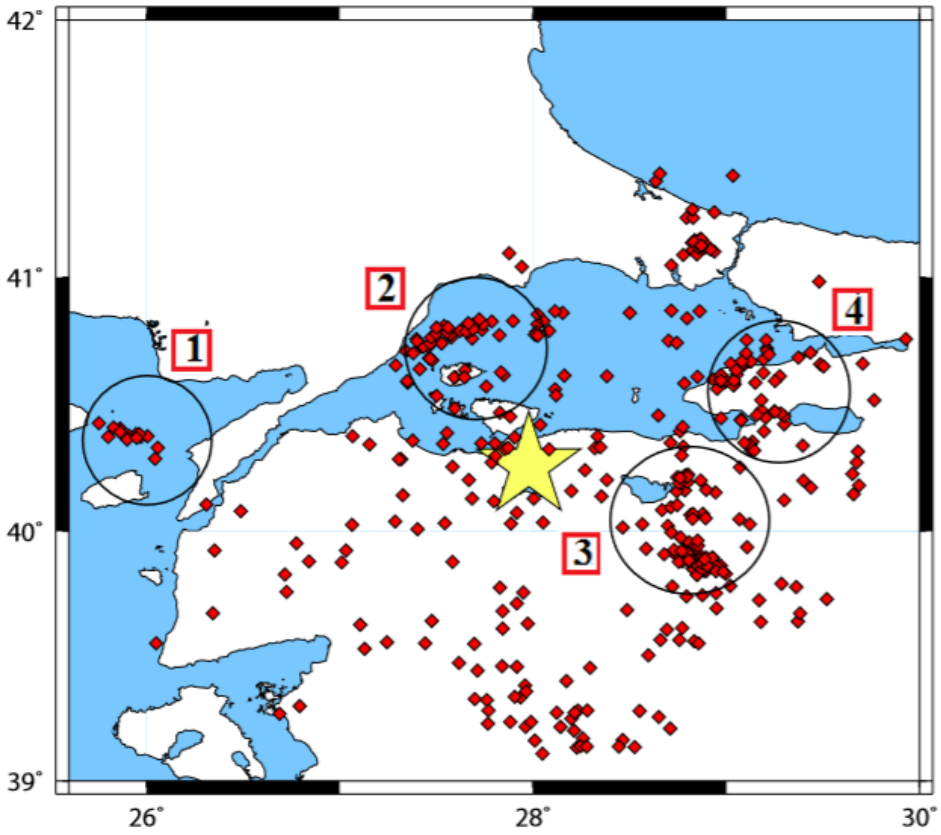

Figure 5.4. Dissemination of microseismic events before the primary earthquake (the primary event: yellow star, microseismic events: red diamonds). Clusters (in black circle) of seismic events utilized in analysis from west to east: (1) Gulf of Saroz; (2) Tekirdag-Murefte; (3) SW Bursa; and (4) Cınarcık-Yalova (see also Figure 2.5).

As stated by these criteria, microseismic events were chosen for each station (Figure 5.5). More than half of the seismic dataset is not utilized because the seismic events are not convenient with the criteria specified previously. An assortment of techniques brings been developed for measuring time-delays and polarizations of shear wave splitting. Plenty of automatic or almost fully automatic techniques have been developed, however, the automatic techniques are not reliable for measuring shear-wave in crustal seismic events because of many shortcomings (Crampin and Gao, 2006). Despite visual techniques are fairly accurate, visual techniques may be not objective and are time consuming. Crampin and peacock (2008) examined basic fallacies in elucidation concerning seismic shear wave splitting of the crustal structure of the Earth. In par-

ticular, the major trouble for determining shear-wave splitting parameters over little earthquakes is that shear-waves have muddled signatures under three component seismograms where the polarizations, and especially time-delays, would intensely scattered and shift generally in time and space (Crampin and Gao, 2006). Cross-correlation system has been utilized by a lot of researchers (e.g., Fukao, 1984; Gao and Zhen, 1995) to identify splitting parameters, in spite of the fact that there would some issues for cross-correlations. A standout amongst those issues may be that it is difficult to make the decision on convenient ends for windows of cross-correlation analysis. On different words, the impact of distinctive endpoints, and distinctive techniques about completion the window might effectively impact those similarly little impacts of shear-wave splitting on a little fragment of the wave-train because of the working of the generally large-amplitude shear and surface-wave coda (Crampin and Gao, 2006). Another issue will be that the waveforms of the fast and slow split shear wave arrivals are not frequently totally comparable.

The comparable issue may be watched for orthogonality between the polarisations of the fast and slow shear wave because they would not totally orthogonal. This demonstrates that direct cross-correlation of autonomous fast and slow shear wave-trains is usually difficult. If microearthquakes happened in the Earth's crust would use, it is could reasonably be expected to watch such issues at almost all surface observations of shear wave splitting. However, such issues would not be observed for teleseismic shear wave splitting because fast and slow shear-waves usually have similar waveforms and also do not have the heavy shear- and surface-wave coda typical of crustal earthquakes. Consequently, it might a chance to be said that cross-correlation method may be a suitable procedure for estimating parameters of shear-wave splitting in the mantle (Silver and Chan, 1988, 1991) that can't constantly make dependably connected to surface observations over earthquakes in the crust. The aspect-ratio technique is also used to measure splitting parameters. Shih et al. (1989) and Shih and Meyer (1990) developed an "aspect-ratio" technique by sequentially rotating seismograms for maximum linearity. This technique is not useful if the time-delays between the shear-waves is a really little. But, Shih et al. (1991) independently calculated time delays by aspect-ratio techniques and by cross-correlating rotated seismograms.

Note that Teanby et al. (2004) utilized the covariance method of silver and Chan (1991) to automatically measure shear-wave splitting from hydrocarbon reservoir-induced events recorded by borehole recorders. As specified above, the subsurface recordings of really little local seismic events were simple signals without near-surface and surface-wave contamination, and the records effectively indicated fleeting changes in shear-wave splitting. In contrast, Peng and Ben-Zion (2004) also utilized the method of silver and Chan (1991) to measure shear-wave splitting in the maintained crustal seismicity along the Karadere–Duzce segment of the NAF in the 6-month period accompanying the 1999 Mw 7. 4 Izmit and Mw 7. 1 Düzce earthquakes. In an endeavor to treat crustal earthquakes, Peng and Ben-Zion (2004) pass the ∼20,000 event data through 10 "objective" quality criteria which left only ∼30% of the records as acceptable data. The shear-wave arrivals begin muddled shear- and surface-wave waveforms and do not have the simplicity of upper mantle arrivals. However, the significant issue is local topography. The majority receivers are located in a relatively narrow valley on the edge of the Almacik Block which rises from ∼100 to ∼1500 m in ∼3 km (Peng and Ben-Zion, 2004). In such irregular topography, the shear-wave polarisations are heavily distorted by topography immediately around the receiver, and the records may be hard to be assessed (Booth and Crampin, 1985; Evans et al., 1987; Crampin and Gao, 2005).

In this study, we determined splitting parameters by utilizing the methods of aspect-ratio, cross-correlation, and systematic analysis of crustal anisotropy (Peng and Ben-Zion, 2004) to acquire definitely high quality splitting parameters. When the results from the methods are compared, it is noticed that the aspect-ratio and cross-correlation are more reliable than the automatic systematic analysis of crustal anisotropy (Peng and Ben-Zion, 2004). Ultimately, such results from the automatic techniques result in making unreliable explanations on orientation and level of anisotropy (Crampin and Peacock, 2008).

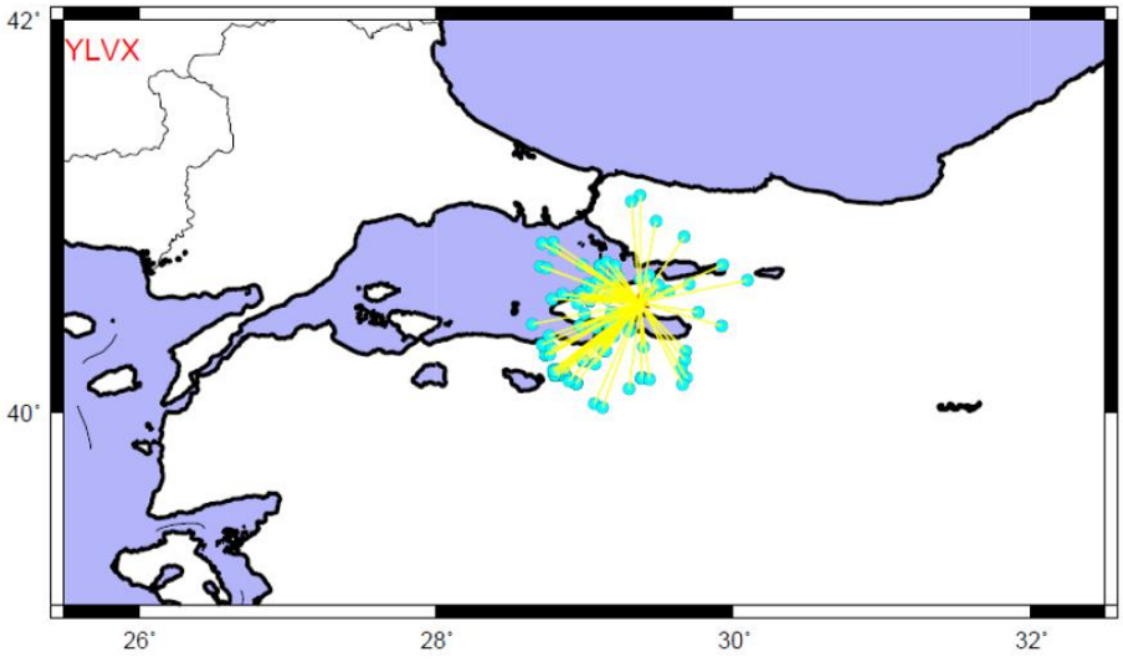

Figure 5.5. The earthquakes are utilized to measure splitting parameters at station YLVX. In total, seismic event distances are smaller than 45 km.

5.2. Results of Splitting Analysis

Robust seismic event groups in the Marmara region (Figure 5.4) before the 2006 Manyas EQ are located in dynamic fault systems in the region (Figure 2.5). We analyzed and relocated seismic event grouping in space and time before and after the 2006 Manyas earthquake in order to reveal the build-up of tension before seismic events and the tension discharge as earthquakes happen. The dissemination of seismic activity in the study region is not uniform in the period January–December 2006. In this way, we inspected the circulation of microearthquakes in longitude and latitude specified in terms of Julian day (day number of a year) and depth to comprehend the principle character of seismic tension in the region (Figure 5.6a, b).

We also inspected the correlation between magnitude and time (Julian day) because we expected changes in magnitude would be identified with time and tension aggregation comparative to the fault system (Figure 5.6c). But, we recognized that

magnitudes of most of the earthquakes are indistinctly less than 3 during 1 year (Figure 5.6c). This means that the magnitudes of the earthquakes did not remarkably change before and after the 2006 Manyas EQ.

Most of the microearthquakes occurred at shallow depths from May 2006 to August 2006 between 27.8^0–29.3^0 longitude and 40^0–40.7^0 latitude. Continuous well-distributed seismic activity was watched during one year-2006 (Figure 5.6a, b, c). Here the goodness of Figure 5.6c fitting a data set comprising of the magnitude and the Julian days of the analyzed seismic events with a fit 1 model is a great visual way to analyze the fitted curve. The bound was characterized by the level of assurance of 95%.

A smooth variation between magnitude and Julian day was watched (Figure 5.6c). As observed in this figure, the proportional connection between magnitude and Julian day is not available. This finding also indicates that it is possible to identify the intricate redistribution of stresses and dynamic strains imposed by the disturbances of the primary event.

In this section of the study, a few stations were chosen in terms of the distances to the primary event so as to see variations in tension before the primary event and analyze them with one other (Figure 5.7a, b, c). In addition to this, as selecting the station, distances between the receivers and event groups were considered (Figure 5.4). Remaining stations except the selected stations were much far from the event groups. Therefore, the seismometers were not chosen for the splitting analysis. The extensive distance between an earthquake and a seismometer may increase the amplitudes of the S phase, this makes difficult to determine correctly the starting and the ending time of the S phase on the waveform.

The distorted S wave relating the high attenuation was thus removed. The seismic event swarm was especially robust during May-2006 (Figure 5.2). Time-delays in Band 1 at station YLVX abruptly diminished almost on May-2006 (Figure 5.7a). By the way, there is however an obvious rise in time-delays in Band-2 at station YLVX

between mid-July and mid-August, 2006 (Figure 5.7a). According to the splitting measurements from 1 January 2006 to 20 October 2006, a spreading behavior in time-delays was obviously observed at station YLVX (Figure 5.7a). From 0 to 25 km, the number of seismic events, additionally bit by bit expanded from January 2006 to 20 October 2006 (Figure 5.6a). This might be related to stress concentration before the 2006 Manyas-Kus Golu earthquake. The average focal depth also little by little enlarged during the period. From 20 July 2006 to 10 October 2006, similar spreading behavior in time-delays is obviously watched at GEMT in spite of the few splitting measurements. Depth range is not stable because of continuous changes in depth parameter of microearthquakes during the period at the surrounding region of the GEMT. The anisotropic pattern in lag times at station YLVX is much like to station GEMT from 20 July 2006 to 10 October 2006 (Figure 5.7a, b). Despite the fact that both stations YLVX and GEMT are located relatively closely, weighted average polarization direction at station GEMT is not comparable to station YLVX (Figure 5.8).

The MRMX station is closer to the 2006 Manyas EQ than the YLVX and GEMT stations. We watched that delay times are almost spreading until mid-July 2006 (Figure 5.7c). The scattering pattern is recognized in the Band-1 and the Band-2. After mid-July 2006, delay times suddenly diminish. However, it is hard to evaluate the observation because our measured parameters are very restricted between May 2006 and mid-July 2006.

Weighted average splitting measurements are also determined for each station utilized in the study. But, for some stations, weighted average splitting parameters are vague for example, ENEZ. This implies that delay times are 0.3s bigger than expected. For such stations, weighted average polarization directions are not indicated on the splitting map (Figure 5.8). In spite of the fact that dissemination of weighted average for per station from microearthquakes is not uniform, most of the weighted average fast polarization directions in the western part of the study are nearly NE-SW but at RKY Station. Weighted average fast polarization directions in eastern Marmara are extremely diffusing (Figure 5.8). In spite of the fact that some stations are located in a small region, their weighted polarization directions are almost perpendicular to

each other (Figure 5.8). The number of microearthquake bit by bit diminished after the primary event. However, some stations, for example, station GEMT, still indicate remarkable changes in delay times (Figure 5.9). Assumed delay times are strikingly increased in Band-2 (Figure 5.9). This might be identified with the area of the station in one of the segments of the NAF (Figure 2.5).

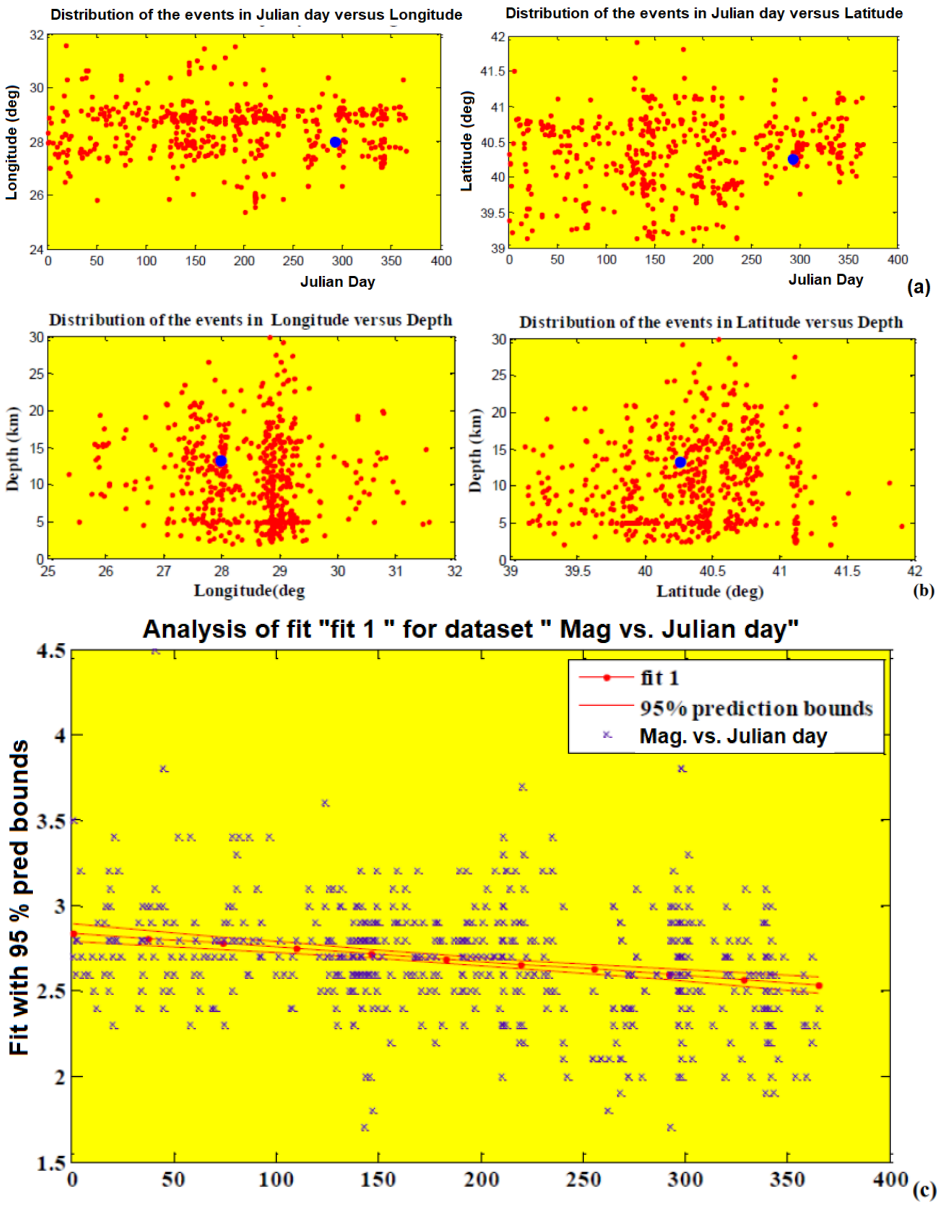

Figure 5.6. (a) Dissemination of microearthquakes in longitude and latitude versus Julian day. Microearthquakes are marked with red dots. The primary earthquake is depicted by a blue circle. (b) Dissemination of microearthquakes in longitude and latitude versus depth. Microearthquakes and the basic earthquake are marked with red dots and blue circle, respectively (c) Analysis of the correlation between magnitude and Julian day.

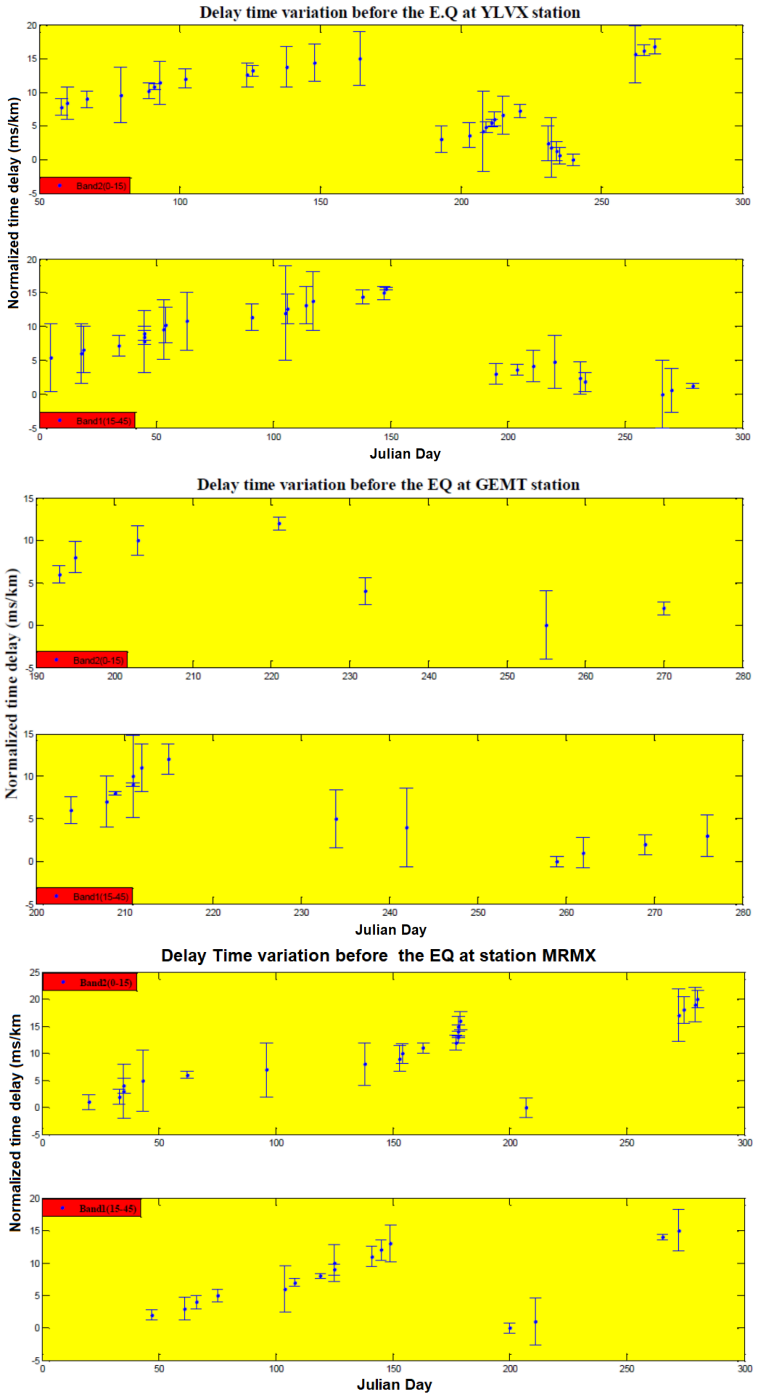

Figure 5.7. (a) Variations of time-delays between split shear waves for 1 January 2006 to 19 October 2006 at station YLVX. (b) Variations of time-delays between split shear waves for 1 January 2006 to 19 October 2006 at station GEMT. (c) Variations of time-delays between split shear waves for 1 January 2006 to 19 October 2006 at station MRMX.

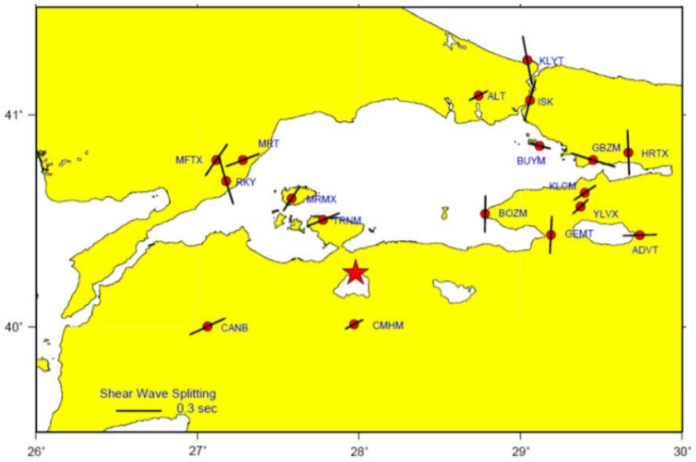

Figure 5.8. Distribution of weighted average results for per station before the main earthquake. The basic event is marked with a red star. Colored bars indicate the fast polarization directions ϕ, which have lengths proportional to the corresponding split time (δt),

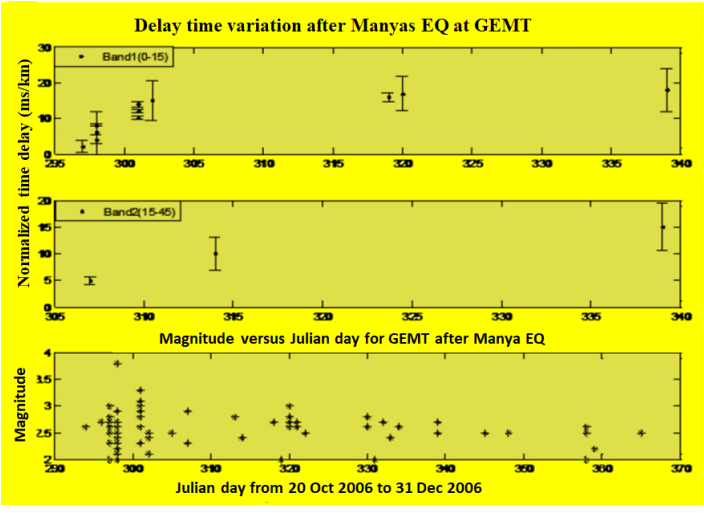

Figure 5.9. Changes in delay time after the primary seismic event at station GEMT. Microearthquakes after the primary seismic event happened. They are marked with asterix.

6. DISCUSSION AND CONCLUSION

Derived results from both methods are discussed. The thesis concludes with a brief summary to draw the main conclusions from the local tomography and shear-wave splitting analysis.

6.1. Discussion on the Results Obtained from the Local Tomography Analysis

The dissemination of seismic velocities acquired from this study is quite compatible with the known tectonic units of the investigated area. P- and S-wave speed anomalies were indicated in Figure 4.4 in four horizontal slices at 5, 15, and 30 km depths and in one vertical section (Figure 4.5). We observed that in most parts of the model, the P and S anomalies are almost like. It may suggest that some contrasts in detail may be clarified by the perplexing structure of the crust in this area. In our case, in the Marmara Sea region, we observed that the crust has a complex structure with seriously modified composition and fracture zones strongly saturated with fluids. For instance, relict igneous blocks are compatible with the measured higher P-velocities. This suggests that the parameter is strongly sensitive to the composition. But, if these rocks were ruptured and saturated with liquid fluids, S-wave velocity would drastically go down. The inverse relationship between the P and S anomalies may be commonly watched in volcanic regions and normally connected with active magma conduits for incompletely liquid rocks (e.g., Koulakov et al., 2013, 2015). In regions of dynamic faults, the correlation between P and S anomalies are basically regulated by the existence of volcanic rocks and the degree of cracking and saturation with liquid or gas fluids. These and several other issues might differently affect the P- and S-velocity and make the P and S anomalies inappropriate

The shallow portion of the crust underneath the Marmara Sea indicates important lateral speed varieties. One of the striking characteristics of this study is that a low-velocity anomaly in the central portion of the Marmara Sea is observed. In addition to

this, high-velocity anomalies the at onshore parts of the study area were found at 5 km depth. At this depth interval, comparatively high P- and S-velocity values at shallow depths were observed in Yalova, Gazikoy, and Tekirdag (Anomalies 1 and 2 in Figure **??**). This finding from this study is fairly compatible with the observed high seismic activity in these regions and the results of Koulakov et al. (2010). Further, high-speed values at the Sakarya Zone and the Armutlu Peninsula were found (Anomaly 3 in Figure **??**). The study of Yılmaz et al. (1995) indicated that the Armutlu Peninsula is ruled by changeable assemblages. Other measured high velocities underneath the Istanbul zone (Anomaly 4 in Figure 4.4), are fairly compatible with a well-developed, unmetamorphosed, and minimal destroyed nonstop Paleozoic sedimentary progression extending from Ordovician to Carboniferous (Ketin, 1973).

In contrast, we found low-velocity values underneath the central part of the Marmara Sea (Anomaly 5 in Figure 4.4), which may be observed particularly in the S-wave speed model at shallow depths. Thus, it could be recommended that this finding may relate of the thick sedimentary stores of the Plio-Pleistocene or of the alluvium districts as underpinned by the low-resistivity and gravity values (Kaya et al., 2013; Bayrakcı et al., 2013). In the Thrace area, we found a negative anomaly in the P and S models (Anomaly 6 in Figure 4.4), compatible with the known geologic composition of the region made of the Late Tertiary store catchment. In the southern portion of Tekirdag Basin, low-velocity values were found at 15 km depth. The finding low-velocity anomalies seem incompatible with active seismicity in the basin and its surrounding area because geological researches (e.g., Okay et al., 1999) indicated that this basin was evaluated in the Pliocene. Due to its comparatively youthful age, the sediments in the basin are not seriously deformed. This finding suggests that there is a subtle connection between the faulting and sedimentation. Comparative characteristics might be a change to be seen in large portions of strike-slip basins, and they often introduce an element of vagueness into the tectonic setting of these basins (Ingersoll and Busby, 1995). Armijo et al. (2005) demonstrated that the area of the Tekirdag Basin had a NW–SE trending transtensional state with nearly purely normal fault mechanisms with some right lateral strike-slip and a few oblique components. Besides, low P and S anomalies (Anomaly 7 in Figure 4.4) were found in the southern part

of the Marmara region, especially Balikesir and Bursa, at the area within the region from 5 and 15 km depths. At these depths, regions with high P-wave velocities are essentially diminished. On the other hand, at these depths, we found that low-velocity areas are little by little diminished. The observed anomalies appear to be strikingly compatible with the known geologic composition of the tectonic structure of the area and the encompassing territory. In recent, Erkan (2015) found moderate heat-flow values in the interior part of the southern Marmara region. As expected, the heat flow strongly affects seismic velocities. This observation appears successfully compatible with, and explains, the low-velocity anomaly (Anomaly 7 in Figure 4.4).

Further, at a depth of 5 km, high P- and S-wave speed varieties were found in the Kuzuluk Basin and encompassing areas. But, Likewise, like patterns in this region were not be found at a depth of 15 km. In the study of the focal mechanism, Tibi et al. (2001) suggested that the west-east extension developed in the Kuzuluk Basin. Besides, some earth scientists (e.g., Greber, 1994; Belin et al., 2002) suggested that several warm wellsprings are compatible with the pull-apart enlargement. A comparative system of the pull-apart basin opening have been previously suggested for the Sea of Marmara (e.g., Armijo et al., 1999; Pondard et al., 2007). Based on the observations from this study, it might be said that the low-speed anomalies found at a depth of 15 km in this area might be identified with the pull-apart basin. At depths of 5 and 15 km, low-velocity anomalies (Anomaly 8 in Figure reffig:figure13) were found underneath the little district between the eastern part of the Izmit Gulf and the Kuzuluk Basin. The findings demonstrate that it may be capable to enlarge the anomaly region up to the sedimentary basins (e.g., Adapazarı, Düzce). However, no further assessments were suggested over the Almacık block due to lack of acceptable and reliable data.

The area between the two segments (the segments indicated B-1 and B-2 in Figure 2.5) of the NAF was defined by comparatively high seismicity (the group of earthquakes primarily located in the branches indicated in Figure 3.4). Looking at the propagation of low and high-speed anomalies in the area, an extensive low-velocity pattern was found underneath the center of the area, in spite of the fact that comparatively high-velocity anomalies were found in the vicinity of the branches. Based on this observation,

it can be said that the finding high-velocity zones are fairly compatible with high resistivity zones (e.g., Tank et al., 2005). In accordance with the study of Tank et al. (2005), these high resistivity zones are also compatible with an asperity that is defined by strong coupling at the fault interface. A similar asperity zone was revealed by Delouis et al. (2000) around the hypocenter in their joint inversion study of InSAR and teleseismic data.

The findings of Nakamura et al. (2002) ve Barış et al. (2005) indicated that the seismic events grouped particularly at the crossing point of low and high-speed zones. This finding appears to be mostly coherent with our findings, but not consistent with the study carried out by Tunç (2008). In accordance with the study of Tunç (2008), mostly seismic events were amassed over low-velocity districts. Additionally, obvious incoherent conduct was observed between the pattern of the P-wave speed of the study of Tunç (2008) and the magnetotelluric research conducted by Tank et al. (2005). However, a strong correlation is observed between S-wave velocity at 10 km to down and the resistivity results produced by Tank et al. (2005).

P-wave velocities in the lower crust underneath the western and southern portions of the Marmara region (e.g., Ganos, Ganos Gulf, Balikesir, Bursa, and the vicinity of the areas indicated in Figure 2.5), under 30 km depth, little by little raise. But, at a depth of 50 km, the P-wave speed extremely reduced (Figure **??**). This might be identified with the truth that the east-west trending normal fault systems of the Sea of Marmara are a scattered zone of the crustal thinning connected with an assumed 30% of north-south expansion since the Tortonian (Ergün et al., 1995). Further, we found that the determination for the S-wave is as well as that for the P-wave. We can thus examine the structure of Vp and Vs in the crust beneath the Marmara region. In spite of the fact that under the depth of 15 km the resolution is not good because of a lack of high-quality seismic events, at a depth of 50 km, for both the P- and S-velocity models, we found a low-velocity anomaly underneath the western part of the Marmara Sea, which may be evaluated as an asthenosphere upwelling. By turns, such upwelling may result in a thermal weakening of the crust that started the process of crustal expansion in the Marmara Sea.

6.2. Discussion on Shear Wave Splitting Results

In this study, a Mb =5.3 Manyas EQ has been retrospectively "stress-forecasted" by utilizing changes in delay times to assess the time and magnitude at which stress-modified micro-fracturing achieves crack criticality within the tensioned volume where strain is discharged. The times and magnitudes of impending big seismic events might be assumed by utilizing such changes in shear-wave splitting since tension induced progressions to microcrack geometry could be monitored by varieties in shear-wave splitting (Crampin and Peacock, 2008). Our determined parameters acquired from microseismic events obviously present the large±80% scatter in time-delays and polarizations that are generally seen above little seismic events (Crampin, 1999) (Figure 5.7a, b, c).

This implies that shear-wave splitting measurements are altogether delicate of the variations over tension. In such studies, one of the fundamental issues is the absence of adequate high-quality seismic events before and after a big seismic event in convenient station-to-seismic event recording geometries. In our study, it is required to mention that azimuthal coverage and density of stations are sufficient and permit us to visualize the variations in splitting measurements. Before the 2006 Manyas EQ, enough insistent swarm activity was observed (Figure 5.2).

The earthquake swarms are significant for stress-forecasting since only such persistent swarms have the capacity to acquire reliable shear wave source signals throughout the build-up of tension. Another crucial point for identifying interim changes in splitting parameters may be existing measurement methods. On the other hand, automatic methods have recently been comprehensively effective (Crampin and Gao, 2006). But, the greater part existing techniques for measuring splitting parameters are inadequate. Therefore, we favored utilizing the visual techniques because they are more reliable than automatic or just about fully automatic methods.

To reduce errors on the measurements caused by free surface and crustal heterogeneity, here three techniques were utilized. Time-delays in seismic shear-wave split-

ting measurements above little seismic events commonly show a scatter of frequently as much as ±80 percent about the mean (Crampin et al., 2004a). The extensive ±80% scatter in time-delays acquired from microseismic events before the primary earthquake at some stations such as station YLVX was observed (Figure 5.7a). However, it was observed that the delay time pattern of MRMX is varied from others (Figure 5.7c). This is most likely explained with the location of the MRMX station (Figure reffig:figure18) because it may be intensively subjected to greater tension than YLVX and others in terms of the high seismic activity in advance of the primary earthquake. The measured splitting parameters at this station become eminently delicate to little variations in stress due to high seismic activity.

Moreover, it may be obviously observed that an M =5 earthquake has the capability to cause variations in splitting measurements that were acquired from a distance of 1000 km (Crampin and Gao, 2010a) because the critical systems of tension-aligned fluid-saturated microfractures affect the sensitivity at distances of hundreds of times the conventional source dimensions. Several seismic events with magnitudes bigger than 3 in the study region happened. This implies that the aggregation of tension has a huge effect on the seismic activity region in advance of the impending earthquake. Merely one event may thus be adequate to visualize the variations in the evaluated parameters. Aggregation of tension around the primary earthquake possesses an important effect on changes in delay times of Band-2. This finding was found at station MRMX. Nearly three months in advance of the 2006 Manyas EQ, undulations in accumulated delay times are noticeable, as observed in Band-2 (0– 15) of station YLVX (Figure 5.7c). As expected that substantial variations in tension cause a rise fracture density underneath the station. Dynamic fault systems and liquid in fracture systems possess additionally an impact on changes in measured splitting parameters. The substantial ±80% scatter and the hypothetical variation of time-delays in Band-1 often hide correlations of time-delays with distance or depth, except for extremely considerable data sets, when averages are significant (Crampin et al., 2004a). The scattering in time delays is related to tension-induced variations in fracture geometry (Figure 5.7a).

In particular, changes in Band-1 for YLVX, MRMX, and GEMT are related to

low-level tension and are exclusively presumable to impress crack aspect ratios which will modify the average time-delay in Band-1 (Figure 5.7a, b, c). The expansive ±80% scatter in time-delays and polarisations at the stations such as YLVX is associated with high pore-fluid pressures on all seismically dynamic fault-planes (Crampin et al., 2004a). The detected anisotropy may come from the upper half or whole upper part of the crust. Sudden variations in delay times and weighted average fast polarization directions between neighboring seismic stations such as YLVX and GEMT may be associated with the localization of anisotropy and implies that it has to be restricted to the near-surface (Crampin and Peacock, 2008).

It is hard to assess the depth range because measured shear-wave time-delays are the accumulated total of the time-delays along the entire of the ray path. We realized that such stress-aligned anisotropy may be uniformly disseminated underneath such depths throughout at least the upper half of the crust but obvious, direct proof of shallow anisotropy is not existing. Despite the weighted average fast polarization at uttermost receivers indicate mostly like a pattern, the dissemination of fast polarization direction is not uniform in the eastern Marmara and the western Marmara (Figure 5.8). The changes in the weighted average fast polarization directions are coherent with the present tectonic structure of the Marmara district. In a fact, the Sea of Marmara is a transition zone between the strike-slip regime of the NAF and the expansion regime of the Aegean Sea (Taymaz, et al., 2004). This probably influences the variations in the determined splitting parameters. After the primary seismic event, we found a clear rise in delay time at station GEMT and seismic activity in the surrounding area that was extremely noticeable (Figure 5.9). Rises in time delays of shear wave splitting monitoring tension aggregation in advance of earthquakes would likewise not precursory to earthquakes. Finally, taking into account variations in splitting parameters before and after the fundamental seismic event, it is difficult to conclude that the location of the forecast seismic event may be forecasted (Jordan et al., 2011). However, we accept that such a study ensures an understanding of how a change in fracture density and fracturing ratio with the aggregation of tension can be noticed at considerable distances from the impending seismic epicentre.

6.3. Summary

The investigated area and the western component of the NAF have a high seismic hazard. These regions are thus of serious importance to seismic events dangers. The target of this Ph.D. thesis was to explore the tectonic structure of the study area utilizing the LET and shear wave splitting. For this, initially, earthquakes from 2005 to 2011 were gathered from continuous and temporary stations installed by the TUBITAK during the TURDEP and KOERI. Later, the gathered local seismic events were relocated. After the relocation of the earthquakes, 2,131 seismic events and an entire of 92,858 arrival times consisting of 50,044 P-wave and 42,814 S-wave arrival times were acquired. The relocated seismic events were processed by utilizing the LOTOS code (Koulakov, 2009) based on iterative inversion. It may be worth specifying that results derived from this analysis indicate that the LET has been effectively used to determine P- and S-wave speed variations for completely the Marmara region. Thus, the detailed crustal form down to a depth of 50 km underneath the Marmara region for P- and S-wave velocities was explored. To reveal critical geodynamical features, the dissemination of obtaining seismic parameters (Vp, Vs) were also taken into account. This investigation demonstrates that the high-speed anomalies quite associate with cracking segments of the NAF. Besides, it may be obviously realized that high seismicity is basically intensified in the branches. In particular, low velocities were found underneath the central Marmara Sea at a depth of 5 km. From 5 to 15 km depth, the existence of velocity varieties between land and the central Marmara Sea was obviously realized. At the depth range from 5 and 15 km, high P- and S-wave velocity values were additionally found underneath the Armutlu Peninsula, Yalova, Gazikoy, and Tekirdağ. In addition to this, high-velocity values in the Sakarya zone were found. Looking at the dissemination of low-speed anomalies, an extensive low-velocity pattern was revealed underneath the central Marmara Sea. We also realized that high-velocity anomalies may be enlarged between the two segments of the NAF and may correlate with the high resistivity zone. On the other hand, we found that the shallow portion of the crust underneath the Marmara Sea indicates noticeable sidewise velocity varieties. The extraordinary feature of this research is that an obvious pattern was found in between the on-land and the central Marmara Sea at the depth range from 5 and 15 km.

In addition to this part of the research, the 2006 Mb =5.3 Manyas-Kus Golu (Manyas) seismic event was retrospectively "stress-forecasted" utilizing changes in time-delays of seismic shear wave splitting to assess the time and magnitude at which stress-modified microcracking attains crack seriousness inside the tensioned volume where strain is discharged.

In addition to this method, the 2006 Mb =5.3 Manyas-Kus Golu (Manyas) earthquake has been retrospectively "stress-forecasted" using variations in time-delays of seismic shear wave splitting to evaluate the time and magnitude at which stress-modified microcracking reaches fracture criticality within the stressed volume where strain is released. We observed that clear decreases in delay times before the impending event, especially at the station GEMT are consistent with the APE model of fluid-rock deformation, but we could not observe similar changes at other stations surrounding the main event. The logarithms of the duration of the stress-accumulation are proportional (selfsimilar) to the magnitude of the impending event. Although time and magnitude of the 2005 Manyas earthquake could have been stress-forecasted, as has been recognized elsewhere, shear wave splitting does not appear to provide direct information about the location of impending earthquakes. We noticed that obvious declines in delay times in advance of the impending seismic event, particularly at the station GEMT are coherent with the APE model of fluid-rock damage, however, we were not able to find like variations at other stations surrounding the major earthquake. The logarithms of the duration of the tension-aggregation are proportional (selfsimilar) to the magnitude of the impending earthquake. Despite time and magnitude of the 2005 Manyas quake were not able to be stress-forecasted, as would have been recognized elsewhere, shear wave splitting does not come out to provide direct evidence about the location of impending earthquakes.

REFERENCES

Adatepe, F., S. Demirel, and B. Alpar, "Tectonic setting of the southern marmara sea region based on seismic reflection data and gravity modelling", *Marine Geology*, 190, pp. 383-395, 2002.

Ambraseys, N.,"The seismic activity of the marmara sea region over the last 2000 years", *Bulletin of the Seismological Society of America*, pp. 1–18, doi:10.1785/0120000843, 2002.

Angerer, E., S. Crampin, X.-Y. Li, and T. L. Davis, "Processing, modelling, and predicting time-lapse effects of over-pressured fluid-injection in a fractured reservoir", *Geophys.* J. Int., pp. 267–280, 2002.

Armijo, R., B. Meyer, A. Hubert, and A. Barka, "Westward propagation of the north anatolian fault into the northern aegean: Timing and kinematics", *Geology*, pp. 267–270, 1999.

Armijo, R., N. Pondard, B. Meyer, B. M. de Lepinay, and G. Ucarkus, "Submarine fault scarps in the sea of marmara pull-apart (north anatolian fault): implications for seismic hazard in istanbul", *Geochemistary Geophysics Geosystems*, p. Q06009, doi:10.1029/2004GC000896, 2005.

Barış, Ş., J. Nakajima, A. Hasegawa, Y. Honkura, A. Ito, and S. B. Ucer, "Three dimensional structure of vp, vs, and vp=vs in the upper crust of the marmara region, nw turkey", *Earth Planets Space*, 57, no. 11, pp. 1019–1038, 2005.

Barka, A. A., "The north anatolian fault zone", *Annual Tectonicae*, pp. 164–195, 1992.

Bayrakcı, G., M. Laigle, A. Becel, A. Hirn, T. Taymaz, S. Yolsal-Cevikbilen, and S. team," 3-D sediment-basement tomography of the northern marmara trough by a dense obs network at the nodes of a grid of controlled source profiles along the

north anatolian fault", *Geophysical Journal International*, 194, pp. 1335–1357, 2013.

Bécel, A., M. Laigle, B. de Voogd, A. H. T. Taymaz, A. Galvé, H. Shimamura, Y. Mura, ´ J. Lepine, M. Sapin, and S. Özalaybey, " Moho, crustal architecture and deep de- ¨ formation under the north marmara trough, from the seismarmara leg1 offshore-onshore reflection-refraction survey", *Tectonophysics*, 467, pp. 1–21, 2009.

Belin B, T. Yalçın, F. Suner, E. Bozkurtoglu, A. Gelir, H. Güven, "Earthquakerelated chemical and radioactivity changes of thermal water in Kuzuluk-Adapazari, Turkey", *J. Env. Radioact*, 63(3):239–249, 2002.

Bianchi, M., B. Heit, A. Jakovlev,X. Yuan, S. M. Kay, E. Sandvol, and D. Comte, "Teleseismic tomography of the southern Puna plateau in Argentina and adjacent regions", *Tectonophysics*, 586, pp. 65-83, 2013.

Bindi, D., S. Parolai, H. Grosser, C. Milkereit, and S. Karakisa, "Crustal attenuation characteristics in northwestern turkey in the range from 1 to 10 hz", *Bull. Seismol. Soc. Am.*, 96, no. 1, pp. 200–214, 2006.

Booth, D. C., and S. Crampin, "Shear-wave polarisations on a curved wavefront at an isotropic free surfaces", *Geophys. J. R. Astr. Soc.*, 83, pp. 31–45, 1985.

Çaka, D.,"Armutlu Yarımadası ve civarında makaslama dalgası ayrımlaşma analizi", *Kocaeli University, Ph.D. thesis*, 2012, unpublished.

Cochran, E. S., J. E. Vidale, and Y.G. Li, "Near-fault anisotropy following the Hector Mine earthquake", *J. Geophys. Res.*, 108, 2436, doi:10.1029/2002JB002352, 2003.

Crampin, S., "Calculable fluid-rock interactions", *J. Geol. Soc.*, pp. 501–514, 1999.

Crampin, S.,"Comment on Local shear wave observations in Joao Camara, northeast Brazil edited by A. F. do Nascimento, R. G. Pearce, and M. K. Takeya,*Journal*

of Geophysical Research (Solid Earth), 109, 2313–+, doi:10.1029/2003JB002681, 2004.

Crampin, S., S. Peacock, Y. Gao, and S. Chastin, " The scatter of time-delays in shear-wave splitting above small earthquakes", *Geophys. J. Int.*, 156, 39–44, 2004a.

Crampin, S., "A second opinion on operational earthquake forecasting: Some thoughts on how and why", edited by thomas jordan and lucille jones, *Seism. Res. Lett*, pp. 227– 230, 2011.

Crampin, S. and Y. Gao, "Comment on "Systematic Analysis of Shear-Wave Splitting in the Aftershock Zone of the 1999 Chi-Chi, Taiwan, Earthquake: Shallow Crustal Anisotropy and Lack of Precursory Changes," by Liu, Teng, and Ben-Zion: Temporal Variations Confirmed", *Bull. Seism. Soc. Am.*, 95, pp. 354-360, 2005.

Crampin, S., and Y. Gao, "A review of techniques for measuring shear-wave splitting above small earthquakes", *Physics of the Earth and Planetary Interiors*, pp. 1–14, 2006.

Crampin, S. and Y. Gao, "Earthquakes can be stress-forecast", *Geophys. J. Int.*, 180, 1124–1127, 2010a.

Crampin, S. and Y. Gao, "A review of a new understanding of fluidrock deformation in the crack-critical crust, in Rock Stress and Earthquakes", *CRC Press*, Taylor-Francs Group, London, 235– 240, 2010b.

Crampin, S., and S. Peacock, "A review of the current understanding of shear-wave splitting and common fallacies in interpretation", *Wave Motion*, pp. 675–722, 2008.

Crampin, S., and S. V. Zatsepin, "Changes of strain before earthquakes: the possibility of routine monitoring of both long-term and short-term precursors", *J. Phys. Earth*, pp. 1–26, 1997.

Crampin, S., Y. Gao, and S. Peacock, "Stress-forecasting (not predicting) earthquakes: A paradigm shift?", *Geology*, pp. 427–430, 2008.

Delouis, B.,P. Lundgren, J. Salichon, D. Giardini, "Joint inversion of InSAR and teleseismic data for the slip history of the 1999 Izmit (Turkey) earthquake", *Geophys Res. Lett.*, 27(20):3389–3392, 2000.

der Sluis, A. V., and H. A. van der Vorst , "Numerical solution of large, sparse linear algebraic systems arising from tomographic problems, in seismic tomography", G. Nolet (editor), Reidel, Dortrecht, pp. 49–83, 1987.

Dewey, J. F., and A. Şengör, "Aegean and surrounding regions complex multiplate and continuum tectonics in a convergent zone", *Geol. Soc. Am. Bull.*, pp. 84–92, 1979.

Ergün, M., E. Özel, C. Sari, " Structure of the Marmara Sea within the North Anatolian Fault zone", In: Banda E, Talwani M, Torne M (eds) NATO ARW book "Ritted ocean-continent boundaries", NATO ASI Series. Kluwer Academic Publishers, Dordrecht, Boston, London, pp. 309–326, 1995.

Erkan, K., "Geothermal investigations in western Anatolia using equilibrium temperatures from shallow boreholes", *Solid Earth*, 6(1), pp. 103–113, 2015.

Evans, R., D. Beamish, S. Crampin, S.B. Üçer, "The Turkish Dilatancy Project (TDP3): multidisciplinary studies of a potential earthquake source region", *Geophys. J. R. Astron. Soc.* 91, pp. 265–286, 1987.

Fukao, Y., " Evidence from core-reflected shear waves for anisotropy in the Earth's mantle", *Nature*, 309(5970), 695, 1984.

Gao, Y., and S. Crampin, "Observations of stress relaxation before earthquakes", *Geophys. J. Int.*, pp. 578–582, 2004.

Gao, Y., P. Wang, S. Zheng, M. Wang, Y. Chen, and H. Zhou, "Temporal changes in shear-wave splitting at an isolated swarm of small earthquakes in 1992 near Dongfang, Hainan Island, southern China, *Geophysical Journal International*, 135, pp. 102–112, 1998.

Gasperini, L., A. Polonia, M. N. C¸ agatay, G. Bortoluzzi, and V. Ferrante, "Geological slip rates along the north anatolian fault in the marmara region", *Tectonics*, doi:10.1029/ 2011TC002906, 2011.

Göncüoğlu, M. C., "Introduction to the geology of turkey: Geodynamic evolution of the pre-alpine and alpine terranes", *MTA Monographs Series.* ISBN 978-605-4075-74, pp. 66, 2010.

Göncüoğlu, M., K. Dirik, and H. Kozlu, "General characteristics of pre-alpine and alpine terranes in turkey: Explanatory notes to the terrane map of Turkey", Annales Geologique de Pays Héllenique, *37 Geol.Soc Greece*, Athens, pp515–536, 1997.

Görür, N., and O. Tüysüz, "Cretaceous to miocene palaeogeographic evolution of Turkey: implications for hydrocarbon potential", *Journ. Petrol. Geol.*, pp. 119–146, 2001.

Greber, E., "Deep circulation of CO2-rich paleowaters in deep seismically active zone (Kuzuluk/Adapazarı, northwestern Turkey)", *Geothermics* 23, pp. 151–174, 1994.

Gürbüz, C., M. Aktar, H. Eyidogan, A. Cisternas, H. Haessler, A. Barka, M. Ergin, N. Turkelli, O. Polat, S. B. Üçer, S. Kuleli, Ş. Barış, B. Kaypak, T. Bekler, E. Zor, F. Biçmen, and A. Yörük, "The seismotectonics of the marmara region (turkey): results from a microseismic experiment", *Tectonophysics*, 316, pp. 1–17, 2000.

Hippolyte, J.-C., N. Espurt, N. Kaymakci, E. Sangu, C. Müller, "Cross-sectional anatomy and geodynamic evolution of the Central Pontide orogenic belt (northern Turkey)", *International Journal of Earth Sciences, Springer Verlag*, 105 (1), pp.

81-106, 2016.

Honkura, Y., and A. M. Işıkkara, "Multidisciplinary research on fault activity in the western part of the north anatolian fault zone", *Tectonophysics*, 193, pp. 347–357, 1991.

Honkura, Y., A. M. Isıkara, D. Kolcak, N. Orbay, S. Sipahioglu, S. Ohshiman, and H. Tanaka ," Magnetic anomalies and low ground resistivity as possible indicators of active fault location: preliminary results of electric and magnetic observations from the western part of the north anatolian fault zone", *J. Geomag. Geoelectr.*, 37, pp. 169–187, 1985.

Honkura, Y., A. M. Isıkara, N. Oshiman, A. Ito, B. Ucer, Ş. Baris, M. K. Tuncer, M. Matsushima, R. Pektas, C. Celik, S. B. Tank, F. Takahashi, R. Yoshimura, Y. Ikeda, and T. Komut , "Preliminary results of multidisciplinary observations before, during and after the kocaeli (izmit) earthquake in the western part of the north anatolian fault zone", *Earth Planets Space*, 52, 293–298, 2000.

Horasan, G., A. Kaslılar-Ozcan, A. Boztepe-Guney, and N. Turkelli, "S-wave attenuation in the marmara region, northwestern turkey", *Geophysical Research Letters*, 25,14, pp. 2733–2736, 1998.

Ingersoll, R.V., C.J. Busby, "Tectonics of sedimentary basins", In: Busby CJ, Ingersoll RV (eds) Tectonics of sedimentary basins. Blackwell Science, Oxford, 1995.

Jackson, J. , "Active tectonics of the aegean region", *Annual Review of Earth and Planetary Sciences*, pp. 239–271, 1994.

Jordan, H., Y. T. Chen, P. Gasparini, R. Madariaga, I. Main, W. Marzocchi, G. P. Papadopoulos, G. A. Sobolev, K. Yamaoka, and J. Zschau, "Operational earthquake forecasting: State of knowledge and guidelines for utilization", *Annals of Geophysics*, pp. 316–391, doi:10.4401/ag-5350, 2011.

Karabulut, H., S. Ozalaybey, T. Taymaz, M. Aktar, O. Selvi, and A. Kocaoğlu, "A tomographic image of the shallow crustal structure in the eastern marmara", *Geophysical Research Letters*, pp. 2277, 2003.

Kaya, T., T. Kasaya, B. Tank, Y. Ogawa, M. Tunçer,N. Oshiman, Y. Honkura, M. Matsushima, " Electrical characterization of the North Anatolian Fault Zone underneath the Marmara Sea, Turkey by ocean bottom magnetotellurics", *Geophys J. Int.*, doi:10.1093/gji/ggt025, 2013.

Ketin, I., "Tectonic units of Anatolia", *Maden Tetkik ve Arama Bulletin*, pp. 23–34, 1966.

Ketin, I., "Bolu –gerede – mengen ve yıgılca bolgesindeki paleozoyik olusuklara ait jeolojik rapor", *TPAO Arama Grubu Rap No:379*, Unpublished (in Turkish), 1967.

Ketin, I., "Genel jeoloji (general geology)", *Published by ITU*, 4th Ed., 1973.

Koulakov, I., M. Bohm, G. Asch, B.-G. Luehr, A.Manzanares, K.S. Brotopuspito, Pak Fauzi, M. A. Purbawinata, N.T. Puspito, A. Ratdomopurbo, H.Kopp, W. Rabbel, E.Shevkunova, " P and S velocity structure of the crust and the upper mantle beneath central Java from local tomography inversion", *J. Geophys. Res.*, 112, B08310, doi:10.1029/2006JB004712, 2007.

Koulakov, I., "LOTOS code for local earthquake tomographic inversion. Benchmarks for testing tomographic algorithms", *Bull. Seismol. Soc. Am.*, 99(1), pp. 194–214. doi:10.1785/0120080013, 2009.

Koulakov, I., D. Bindi, S. Parolai, H. Grosser, and C. Milkereit, "Distribution of seismic velocities and attenuation in the crust beneath the north anatolian fault (turkey) from local earthquake tomography", *Bull. Seismol. Soc. Am.*, 100, pp. 207–224. doi: 10.1785/0120090105, 2010.

Koulakov I, M. West, P. Izbekov, "Fluid ascent during the 2004–2005 unrest at Mt.

Spurr inferred from seismic tomography", *Geophys Res. Lett.* 40(17):4579–4582. doi:10.1002/grl.50674, 2013.

Koulakov I, S. El Khrepy, N. Al-Arifi, P. Kuznetsov, E. Kasatkina, "Structural cause of a missed eruption in the Harrat Lunayyir basaltic field (Saudi Arabia) in 2009", *Geology*, G36271:1. doi:10.1130/G36271.1, 2015.

Laigle, M., A. Becel, B. de Voogd, A. Hirn, T. Taymaz, S. Ozalaybey, M. of SEIS-MARMARA Leg1 Team, "A first deep seismic survey in the sea of marmara: Deep basins and whole trust architecture and evolution", *Earth and Planetary Science Letters*, 270(3-4) pp. 168–179, 2008.

Lee, W. H. K., and J. C. Lahr, "Hyp071 (revised): a computer program for determining hypocenter, magnitude, and first motion pattern of local earthquakes", *U. S. Geological Survey Open File Report*, pp. 75–311, 1975.

McClusky, S., S. McClusky, S. Balassanian, A. Barka, C. Demir, S. Ergintav, I. Georgiev, O. Gurkan, M. Hamburger, K. Hurst, H. Kahle, K. Kastens, G. Kekelidze, R. King, V. Kotzev, O. Lenk, S. Mahmoud, A. Mishin, M. Nadariya, A. Ouzounis, D. Paradissis, Y. Peter, M. Prilepin, R. Reilinger, I. Sanli, H. Seeger, A. Tealeb, M. N. Toksoz, and ¨ G. Veis, "Global positioning system constraints on plate kinematics and dynamics in the eastern mediterranean and caucasus", *Journal of Geophysical Research*, pp. 5695– 5719, 2000.

McKenzie, D. P., "Active tectonics of the mediterranean region", *Geophys. J. R. Astron. Soc.*, pp. 109–185, 1972.

Meade, B. J., B. H. Hager, and R. E. Reilinger, "Estimates of seismic potential in the marmara region from block models of secular deformation constrained by gps measurements", *Bull. Seism. Soc. Am.*, pp. 208–215, doi:10.1785/0120000837, 2002.

Nakamura, A., A. Hasegawa, A. Ito, S. B. Ucer, S. Baris, Y. Honkura, T. Kono, S. Hori,

R. Pektas, T. Komut, C. Celik, and A. M. Isikara, "P-wave velocity structure of the crust and its relationship to the occurrence of the 1999 izmit, Turkey earthquake and aftershocks", *Bull. Seism. Soc. Am.*, pp. 330–338, 2002.

Okay, A. I., "Tectonics units and sutures in the pontides, northern Turkey, Tectonic evolution of the Tethyan Region", *Nato ASI Series., Series C*, 259, 109–116, 1986.

Okay, A. I., E. Demirbağ, H. Kurt, N. Okay, I. Kusçu, "An active, deep marine strike-slip basin along the North Anatolian fault in Turkey", *Tectonics*, 18:129–148, 1999.

Okay, A. I., "Geology of Turkey: A synopsis", *Anschnitt*, pp. 19–42, 2008.

Okay, A. I., A. Kaşlılar-Ozcan, C. Imren, A. Boztepe-Guney, E. Demirbağ, and I. Kuşcu , Active faults and evolving strike-slip basins in the marmara sea, northwest turkey: a multichannel seismic reflection study, *Tectonophysics*, 321, 189–218, 2000.

Onder Cetin, K., N. Isik, B. Unutmaz, "Seismically induced landslide at Degirmendere Nose, Izmit Bay during Kocaeli (Izmit)-Turkey earthquake, *Soil Dyn Earthq Eng* 24, pp. 189–197, 2004.

Paige, C., and M. A. Saunders, "Lsqr: An algorithm for sparse linear equations and sparse least squares, Association for Computing Machinery", *Transactions on Mathematical Software*, 8, pp. 43–71, doi:10.1145/355984.355989, 1982.

Peng, Z. and Y. Ben-Zion, "Systematic analysis of crustal anisotropy along the Karadere–Duzce branch of the North Anatolian fault", *Geophys. J. Int.*, 159, 253–274, 2004.

Peacock, S., S. Crampin, D. C. Booth, and J. B. Fletcher, "Shear wave splitting in the Anza seismic gap, southern California: Temporal variations as possible precursors", *Journal of Geophysical Research*, 93, pp. 3339–3356, doi:10.1029/88JB01319, 1988.

Pichon, X. L., N. Chamot-Rooke, and S. Lallemant, "Geodetic determination of the kinematics of central greece with respect to europe: Implications for eastern mediterranean tectonics", *Journal of Geophysical Research*, pp. 675–690, 1995.

Polat, G., N. M. Ozel, S. Crampin, S. Ergintav, and O. Tan, "Shear wave splitting as a proxy for stress forecast of the case of the 2006 manyas-kus golu (mb = 5.3) earthquake", *Nat. Hazards Earth Syst. Sci.*, pp. 1073–1084, doi:10.5194/nhess-12-1073-2012, 2012.

Pondard N, R. Armijo, G.C.P. King, B. Meyer, F. Flerit, "Fault interactions in the Sea of Marmara pull-apart (North Anatolian fault): earthquake clustering and propagating earthquake sequences", *Geophys J. Int.* 171:1185–1197 , 2007.

Reillinger, R., S. McClusky, P. Vernant, S. Lawrence, S. Ergintav, H. O. R. Cakmak, F. Kadirov, I. Guliev, R. Stepanyan, M. Nadariya, G. Hahubia, S. Mahmoud, K. Sakr, A. ArRajehi, D. Paradissis, A. Al-Aydrus, M. Prilepin, T. Guseva, E. Evren, A. Dmitrotsa, S. Filikov, F. Gomez, R. Al-Ghazzi, and G. Karam, "Gps constraints on continental deformation in the africa-arabia-eurasia continental collision zone and implications for the dynamics of plate interactions", *Journal of Geophysical Research*, doi: 10.1029/2005JB004051, 2006.

Salah, M. K., S. Sahin, and M. Kaplan, "Seismic velocity structure along the western segment of the north anatolian fault zone imaged by seismic tomograph", *Bull. Earthq. Res. Inst. Univ. Tokyo*, 82, pp. 209–223, 2007.

Şaroğlu, F., O. Emre, and A. Boray, "Turkiye'nin diri fayları ve depremsellikleri", Maden Tetkik ve Arama Genel Müdürlüğü jeoloji etüdleri dairesi başkanlığı, Ankara ili +394 s.+11 harita, 1987.

Schmittbuhl, J., H. Karabulut, O. Lengline, and M. Bouchon, "Seismicity distribution and locking depth along the main marmara fault, Turkey", *Geochem. Geophys. Geosyst.*, doi:10.1002/2015GC00612, 2015.

Şengör, A. M. C., and Y. Yılmaz, "Tethyan evolution of Turkey: a plate tectonic approach", *Tectonophysics*, 75, pp. 181–241, 1981.

Şengör, A. M. C., and Y. Yılmaz, "Tethyan evolution of Turkey: A plate tectonic approach", *Tectonophysics*, pp. 181–241, 1995.

Shih X.R.,R. P. Meyer, J.F. Schneider, "An automated, analytical method to determine shear-wave splitting", *Tectonophysics*, 165, pp. 271–278, 1989.

Shih, O. R. and P. R. Meyer, "Observation of Shear Wave Splitting From Natural Events "South Moat of Long Valley Caldera", California, June 29 to August 12, 1982, *J. Geophys. Res.*, 95, 11179–11195, 1990.

Shih X.R., J.F. Schneider,R.P. Meyer, "Polarities of P and S waves, and shear wave splitting observed from the Bucaramanga Nest Columbia", *J. Geophys. Res.*, 96, pp. 12069–12082, 1991.

Silver, P.G. and W.W. Chan, " Implications for continental structure and evolution from seismic anisotropy", *Nature*, 335, pp. 34-39, 1988.

Silver, P.G. and W.W. Chan, " Shear-wave splitting and subcontinental mantle deformation", *J. geophys. Res.*, 96, vol:16, pp. 429- 454, 1991.

Smith, A., F. Oktay, T. Taymaz, J. Jackson, H. Başaran, B. Alpar, M. Şimşek, and S. Kara , "High resolution of seismic profiling in the sea of marmara-nw turkey: late quaternary sedimentation and sea-level changes", *GSA Bull.*, pp. 923–936, 1995.

Straub, C., H. G. Kahle, and C. Schindler, Gps and geologic estimates of the tectonic activity in the marmara sea region, nw anatolia, *Journal of Geophysical Research*, pp. 587–601, doi:10.1029/97JB02563, 1997.

Tank, B., Y. Honkura, Y. Ogawa, M. Matsushima, N. Oshiman, M.K. Tunçer, C. Çelik, E. Tolak, A.M. Işkıkara, "Magnetotelluric imaging of the fault rupture area of

the 1999 İzmit (Turkey) earthquake", *Phys Earth Planet Inter*, 150(1–3):213–225, 2005.

Taymaz T., R. Westaway, R. Reilinger, "Active faulting and crustal deformation in the Eastern Mediterranean Region", *Tectonophysics* , vol. 391, pp. 1–4, 375 doi:10.1016/j.tecto.2004.07.005, 2004.

Taymaz, T., O. Tan, and S. Yolsal, "Recent Devastating Earthquakes in Turkey and Active Tectonics of the Aegean and Marmara Seas, Earthquake Monitoring and Seismic Hazard Mitigation in Balkan Countries", *NATO Science Series: IV: Earth and Environmental Sciences*, 81, II, 47–55, doi:10.1007/978-1-4020- 6815-7 3, 2008.

Teanby, N., J.-M. Kendall, R. H. Jones, and O. Barkved, "FAST TRACK PAPER: Stress induced temporal variations in seismic anisotropy observed in microseismic data", *Geophysi cal Journal International*, 156,pp. 459–466, doi:10.1111/j.1365-246X.2004.02212.x., 2004.

Thurber, C.H., "Earthquake locations and three-dimensional crustal structure in the Coyote Lake area, central California", *Journal of Geophysical Research*, 88:8226–8236, 1983.

Tibi, R., G. Bock, Y. Xia, M. Baumbach, H. Grosser, C. Milkereit, S. Karakisa, S. Zübül,R. Kind, J. Zschau, Rupture processes of the August 17 İzmit and November 12, 1999, Düzce (Turkey) earthquakes", *Geophys. J. Int.*, 144(2):F1–F7, 2001.

Tunç, B.,"Marmara bölgesi'nin üç-boyutlu hız yapısının sismik tomografi yöntemleri ile belirlenmesi", *Kocaeli University, Ph.D. thesis*, 2008, unpublished.

Volti, T., and S. Crampin, "A four-year study of shear-wave splitting in iceland: 1. background and preliminary analysis, in new insights into structural interpretation and modelling".: edited by D.A. Nieuwland, *Geol. Soc. Lond.*, pp. 117–133, 2003a.

Volti, T., and S. Crampin, "A four-year study of shear-wave splitting in iceland: 2.

temporal changes before earthquakes and volcanic eruptions, in new insights into structural interpretation and modelling" edited by D.A. Nieuwland, *Geol. Soc. Lond.*, pp. 135–149, 2003b.

Yılmazer, M., "ZsacWin (kandilli earthquake processing software) is developed for koeri: http://www.koeri.boun.edu.tr/.", 2003.

Yılmaz, Y., S. C. Genc, E. Yigitbas, M. Bozcu, and K. Yılmaz, "Geological evolution of the late mesozoic continental margin of the north western anatolia", *Tectonophysics*, pp. 155–171, 1995.

Zatsepin, S. V., and S. Crampin, " Modelling the compliance of crustal rock: I - response of shear-wave splitting to differential stress", *Geophys. J. Int.*, pp. 477–494, 1997.